T cell priming is enhanced by maturation-dependent stiffening of the dendritic cell cortex

Daniel Blumenthal, Lyndsay Avery, Vidhi Chandra, and Janis K. Burkhardt*

Department of Pathology and Laboratory Medicine,

Children's Hospital of Philadelphia Research Institute and

Perelman School of Medicine at the University of Pennsylvania,

Philadelphia, PA, USA

*Correspondence:
Janis K. Burkhardt
Department of Pathology and Laboratory Medicine
Children's Hospital of Philadelphia Research Institute
3615 Civic Center Blvd, ARC 815D,
Philadelphia, PA 19104, USA
Tel: 267-426-5410
E-mail: jburkhar@pennmedicine.upenn.edu

Running Title: Modulation of T cell activation by dendritic cell cortical stiffness

Key Words: actin, mechanotransduction, maturation, costimulation, signaling, cytoskeleton

ABSTRACT

T cell activation by dendritic cells (DCs) involves forces exerted by the T cell actin cytoskeleton, which are opposed by the cortical cytoskeleton of the interacting APC. During an immune response, DCs undergo a maturation process that optimizes their ability to efficiently prime naïve T cells. Using atomic force microscopy, we find that during maturation, DC cortical stiffness increases via process that involves actin polymerization. Using stimulatory hydrogels and DCs expressing mutant cytoskeletal proteins, we find that increasing stiffness lowers the agonist dose needed for T cell activation. $CD4^+$ T cells exhibit much more profound stiffness-dependency than $CD8^+$ T cells. Finally, stiffness responses are most robust when T cells are stimulated with pMHC rather than anti-CD3ε, consistent with a mechanosensing mechanism involving receptor deformation. Taken together, our data reveal that maturation-associated cytoskeletal changes alter the biophysical properties of DCs, providing mechanical cues that costimulate T cell activation.

14 **INTRODUCTION**

15 The initiation of an adaptive immune response requires priming of naïve T cells by professional
16 antigen presenting cells (APCs). This process involves multiple receptor-ligand interactions,
17 which occur in concert at a specialized cell-cell contact site called the immunological synapse
18 (Dustin, 2014). Through these interactions, APCs transmit a highly orchestrated series of signals
19 that induce T cell activation and direct differentiation of T cell populations (Friedl, den Boer, &
20 Gunzer, 2005). While the biochemical aspects of this process have been the subject of many
21 studies, the contribution of mechanical cues is only now being uncovered.

22 Following initial T cell receptor (TCR) engagement, T cells apply pushing and pulling forces on
23 interacting APCs (Bashour et al., 2014; Hui, Balagopalan, Samelson, & Upadhyaya, 2015; Husson,
24 Chemin, Bohineust, Hivroz, & Henry, 2011; Sawicka et al., 2017). These forces are essential for
25 proper T cell activation (Li et al., 2010; Pryshchep, Zarnitsyna, Hong, Evavold, & Zhu, 2014).
26 Moreover, force application is responsible, at least in part, for the ability of T cells to rapidly
27 discriminate between agonist and antagonist antigens (Das et al., 2015; Liu, Chen, Evavold, &
28 Zhu, 2014). While the mechanism by which force is translated into biochemical cues remains
29 controversial (Das et al., 2015; Hong et al., 2015; Kim et al., 2009), there is evidence that early
30 tyrosine phosphorylation events downstream of TCR engagement occur at sites where applied
31 force is maximal (Bashour et al., 2014). Interestingly, the amount of force a T cell applies is
32 directly affected by the stiffness of the stimulatory substrate (Husson et al., 2011; Sawicka et al.,
33 2017). Thus, it appears that force application is mechanically coupled to the T cell's ability to
34 sense stiffness (mechanosensing). In other cell types, substrate stiffness has been shown to
35 affect a variety of cell functions including differentiation, migration, growth and survival (Byfield,
36 Reen, Shentu, Levitan, & Gooch, 2009; Discher, Janmey, & Wang, 2005; Engler, Sen, Sweeney, &
37 Discher; Lo, Wang, Dembo, & Wang; Oakes et al., 2009; Pelham & Wang, 1997; Solon, Levental,

38 Sengupta, Georges, & Janmey; Trappmann et al., 2012). Stiffness sensing in T cells has not been
39 well studied, though there is some evidence that substrate stiffness affects both initial priming
40 and effector functions (Basu et al., 2016; Judokusumo, Tabdanov, Kumari, Dustin, & Kam, 2012;
41 O'Connor et al., 2012; Saitakis et al., 2017). Since the physiologically relevant substrate for T cell
42 priming is the surface of the interacting APC, one might predict that changes in cortical stiffness
43 of the APC will profoundly influence T cell priming. However, this prediction remains untested,
44 and studies addressing the role of substrate stiffness in T cell priming did not take into
45 consideration the physiological stiffness of APCs.

46 Dendritic cells (DCs) are the dominant APCs that prime T cells *in vivo* (Jung et al., 2002). One of
47 the hallmarks of DC biology is the process of maturation. Immature DCs are sentinels of the
48 immune system, specialized for immune surveillance and antigen processing (Mellman &
49 Steinman, 2001). In response to infection or injury, inflammatory stimuli trigger signaling
50 pathways that induce molecular reprogramming of the cell. The resulting mature DCs express
51 high levels of surface ligands and cytokines needed for efficient T cell priming (Burns et al.,
52 2004). The maturation process is tightly associated with remodeling of the DC actin
53 cytoskeleton. This process underlies other maturation-associated changes such as
54 downregulation of endocytosis and increased migratory behavior (Garrett et al., 2000; West,
55 Prescott, Eskelinen, Ridley, & Watts, 2000). In addition, cytoskeletal remodeling has a direct
56 impact on the ability of mature DCs to prime T cells (Al-Alwan, Rowden, Lee, & West, 2001;
57 Comrie, Li, Boyle, & Burkhardt, 2015). Indeed, depolymerization of actin filaments perturbs the
58 ability of mature peptide-pulsed DCs to activate T cells, indicating that actin plays an important
59 role on the DC side of the immunological synapse. We hypothesized that maturation-associated
60 changes in the actin cytoskeleton modulate the stiffness of the DC cortex, and promote T cell

61 priming by providing physical resistance to the pushing and pulling forces exerted by the
62 interacting T cell.

63 In this work, we aimed to better understand the relationship between DC cortical stiffness and T
64 cell activation. We show that during maturation, DCs undergo a 2-3 fold increase in cortical
65 stiffness, and that T cell activation is sensitive to stiffness over the same range. Moreover, we
66 find that stiffness sensitivity is a general trait exhibited by most T cell populations. Since
67 mechanosensing occurs lowers the threshold signal required for T cell activation, we conclude
68 that stiffness serves as a novel biophysical costimulatory mechanism that functions in concert
69 with canonical signaling cues to facilitate T cell priming.

70 **RESULTS**

71 **Dendritic cell stiffness increases upon maturation.**

72 During maturation, DCs undergo a set of phenotypic changes that transform them into highly
73 effective APCs (Mellman & Steinman, 2001). We hypothesized that as part of this maturation
74 process, DCs might also modulate their cortical stiffness. To test this, we used atomic force
75 microscopy (AFM) to directly measure cortical stiffness of immature and mature DCs. Murine
76 bone marrow derived DCs (BMDCs) were prepared as described in Materials and Methods and
77 cultured in the absence or presence of LPS to induce maturation. Cells were plated on Poly L-
78 lysine (PLL) coated coverslips and allowed to spread for at least 4 hours prior to measurement of
79 cortical stiffness by AFM micro-indentation. Because the population of LPS-treated cells was
80 heterogeneous with respect to maturation markers, cells were labeled with fluorescent anti-
81 CD86, and immature (CD86-negative) or mature (CD86 high) cells were selected for AFM
82 measurements. As shown in Figure 1A, immature BMDCs were quite soft, with a mean Young's
83 modulus of 2.2±0.7 kPa. Mature BMDCs were almost two-fold stiffer, with a Young's modulus of
84 3.5±1.0 kPa. Importantly, the stiffness of CD86-negative BMDCs within the LPS-treated population
85 was the same as that of untreated, immature DCs. This demonstrates that the observed increase
86 in stiffness is a property of DC maturation rather than an unrelated response to LPS treatment.
87 Since BMDCs do not recapitulate all of the properties of classical, tissue resident DCs (Guilliams &
88 Malissen, 2015; Lutz, Inaba, Schuler, & Romani, 2016; Na, Jung, Gu, & Seok, 2016), we verified our
89 results by measuring the stiffness of *ex-vivo* DCs purified from spleens of untreated or LPS-injected
90 mice. Results were very similar; the stiffness of immature splenic DCs was nearly identical to that
91 of immature BMDCs, and LPS treatment resulted in an increase in stiffness of almost 3-fold (Figure
92 1B). These results demonstrate that stiffness modulation is a *bona fide* trait of DC maturation.
93 Moreover, they establish that the biologically relevant range of DC stiffness lies between 2 and 8
94 kPa.

95 **The maturation-induced increase in stiffness is actin dependent and substrate independent.**

96 One well-known feature of DC maturation is remodeling of the actin cytoskeleton. This process
97 involves changes in the activation status of Rho GTPases and downstream actin regulatory
98 proteins, and is known to downregulate antigen uptake and increase cell motility (Garrett et al.,
99 2000; West et al., 2000). To ask if changes in actin cytoarchitecture also result in increased cortical
100 stiffness, we treated immature and mature BMDCs with the actin-depolymerizing agents
101 Cytochalasin-D or Latrunculin-B. Neither drug affected the stiffness of immature BMDCs,
102 indicating that the basal level of stiffness depends on factors other than the actin cytoskeleton
103 (Figure 1C). In contrast, both drugs induced a significant decrease in the stiffness of mature DCs,
104 with Cytochalasin reducing their stiffness to that of immature DCs. We conclude that the
105 increased cortical stiffness observed upon DC maturation is another feature of actin cytoskeletal
106 reprogramming.

107 Some cell types regulate their stiffness in response to the stiffness of their substrate (Byfield et
108 al., 2009; Tee, Fu, Chen, & Janmey, 2011). To test whether DCs exhibit this behavior, immature
109 and mature BMDCs were plated on PLL-coated substrates of different compliances (hydrogels of
110 2 or 25 kPa, or glass surfaces in the GPa range) and allowed to spread on the surface for at least
111 4 hours prior to AFM measurement. No apparent difference in cell spreading or morphology could
112 be noted on the different PLL-coated hydrogels (data not shown). Hydrogel compliance was
113 verified by measuring the elastic modulus of the surface in areas devoid of cells (Figure 1 - Figure
114 Supplement 1). As shown in Figure 1D, substrate compliance had no effect on cortical stiffness of
115 either immature or mature BMDCs. In control studies, we could readily detect substrate-
116 dependent changes in stiffness of normal fibroblast cells (not shown). Thus, we conclude that DCs
117 maintain a specific cortical stiffness, which is characteristic of their maturation state.

118 **DC cortical stiffness is primarily controlled by actin polymerization**

119 We next sought to identify the molecular mechanisms controlling DC cortical stiffness. Several
120 actin regulatory mechanisms are known to change during DC maturation. In particular, mature
121 DCs upregulate the actin bundling protein fascin (Yamashiro, 2012), they show activation of
122 myosin-dependent processes (van Helden et al., 2008), and they undergo changes in the
123 activation and localization of Rho-GTPases, which in turn regulate actin polymerization via the
124 Arp2/3 complex and formins (Burns, Thrasher, Blundell, Machesky, & Jones, 2001; Garrett et al.,
125 2000; West et al., 2000). To ask how each of these pathways influences cortical stiffness, we used
126 small molecule inhibitors and DCs from relevant knockout mice. Note that to facilitate comparison
127 between experiments, control immature and mature DCs were tested in each experiment, and
128 results were normalized based on values for mature DCs. First, we tested the role of fascin, which
129 is known to generate very stiff actin bundles *in vitro* (Demoulin, Carlier, Bibette, & Baudry, 2014).
130 Surprisingly, the stiffness of BMDCs from fascin$^{-/-}$ mice was indistinguishable from that of WT
131 BMDCs both before and after LPS-induced maturation (Figure 2A). Next, we tested the
132 contribution of myosin contractility, which is known to control stiffness and membrane tension in
133 other cell types (Salbreux, Charras, & Paluch, 2012). As shown in Figure 2B, treating mature
134 BMDCs with the myosin II inhibitor blebbistatin reduced stiffness by a small, albeit statistically
135 significant amount. Similar results were obtained with the Rho-kinase (ROCK) inhibitor Y27623,
136 which indirectly inhibits myosin function.

137 We next considered the possibility that cortical stiffness is modulated by actin polymerization.
138 Broadly speaking, actin polymerization is induced by two sets of proteins: formins generate linear
139 actin filaments, while activators of the Arp2/3 complex produce branched actin structures.
140 Treatment of DCs with the pan-formin inhibitor SMIFH2 significantly reduced the cortical stiffness
141 of mature DCs (Figure 2B). A similar reduction was observed after inhibition of Arp2/3-mediated
142 branched actin polymerization by CK666. DCs express multiple activators of Arp2/3 complex, of

143 which two have been implicated in maturation-associated changes in actin architecture:
144 Hematopoietic Lineage Cell-Specific Protein 1 (HS1), the hematopoietic homologue of cortactin
145 (Huang et al., 2011), and WASp, the protein defective in Wiskott-Aldrich syndrome (Bouma, Burns,
146 & Thrasher, 2007; Bouma et al., 2011; Calle, Chou, Thrasher, & Jones, 2004). To individually assess
147 the role of these two proteins, we used BMDCs cultured from HS1 and WASp knockout mice. As
148 shown in Figure 2A, loss of HS1 had no impact on cortical stiffness of either immature or mature
149 BMDCs. In contrast, mature WASp knockout BMDCs were significantly less stiff than WT controls.
150 This difference mirrors that seen after inhibition of Arp2/3 complex by CK666, suggesting that
151 WASp is the primary activator of Arp2/3 complex-dependent changes in cortical stiffness. The
152 defect in WASp knockout DCs was observed only after maturation; immature WASp knockout DCs
153 did not differ in stiffness from WT controls. This is consistent with our finding that the stiffness of
154 immature DCs is unaffected by actin depolymerizing agents. Taken together, these results show
155 that activation of formin and WASp-dependent actin polymerization pathways, and to a lesser
156 extent increased myosin contractility, all contribute to the increased cortical stiffness of mature
157 DCs.

158 **Stiffness lowers the threshold for activation of CD4$^+$ T cells, but not CD8$^+$ T cells.**

159 Our findings raise the possibility that changes in DC cortical stiffness, like other maturation-
160 induced changes, enhance the ability of these cells to prime a T cell response. Previous studies
161 have shown that T cells are sensitive to the stiffness of stimulatory surfaces (Judokusumo et al.,
162 2012; O'Connor et al., 2012), and that that the TCR serves as the mechanosensory (Judokusumo
163 et al., 2012). However, the results are conflicting, and these earlier studies were not performed
164 within the physiological stiffness range that we have defined for DCs. Thus, we tested T cell
165 responses on hydrogels with a stiffness range spanning that of immature and mature DCs (2 – 25
166 kPa). We verified the compliance of the hydrogel surfaces by measuring the elastic modulus of

167 the surfaces directly by AFM. Hydrogel stiffnesses were found to be similar to those reported by
168 the manufacturer (Figure 3 - Figure Supplement 1). Surfaces were coated with varying doses of
169 peptide-loaded major histocompatibility complex (pMHC) molecules, together with a constant
170 dose of anti-CD28. Surfaces were coated with H-2K^b class I MHC loaded with the N4 (SIINFEKL)
171 peptide (pMHC-I), or I-A^b class II MHC loaded with the OVA$_{329-337}$ (AAHAEINEA) peptide (pMHC-
172 II), to stimulate OT-I CD8$^+$ or OT-II CD4$^+$ T cells, respectively. Plastic surfaces, which are commonly
173 used for stimulation with surface-bound ligands, were included as a familiar reference point. To
174 test the effects of substrate stiffness on early T cell activation, we measured surface expression
175 of the activation markers CD25 and CD69, as well as the production of IL-2, all at 24 hours post
176 stimulation. As shown in Figure 3A-C, CD4$^+$ T cells showed a profound stiffness-dependent
177 response at 24 hours across all measures. This response was most clearly seen for upregulation
178 of CD25 and CD69, where increasing substrate stiffness enhanced the CD4+ T cell response in a
179 graded manner. As expected, for any given substrate stiffness T cell activation increased with
180 increasing peptide dose. However, comparison between stimulatory surfaces revealed that
181 increasing substrate stiffness lowered the pMHC-II dose required to obtain the same level of
182 activation. Over the stiffness range associated with DC maturation (2-8kPa), the dose of TCR signal
183 needed to induce surface marker upregulation was shifted by 1-2 logs. Analysis of IL-2 production
184 revealed a similar effect, although the stiffness sensitivity was more bi-modal. IL-2 production
185 increased almost 3-fold when CD4+ T cells were stimulated on surfaces of 8kPa, as opposed to
186 2kPa, for the same antigen dose.

187 Strikingly, the robust stiffness response we observed in CD4$^+$ T cells was not recapitulated for CD8$^+$
188 T cells, especially when T cell activation was assessed based on surface marker upregulation
189 (Figure 3D,E). Analysis of IL-2 production did reveal stiffness-enhanced activation of naïve CD8$^+$ T

190 cells, but this was largely restricted to substrates outside the stiffness range defined for DCs
191 (12kPa, 25 kPa and plastic).

192 To determine if the stiffness dependency of $CD4^+$ T cells seen at early times after TCR engagement
193 is maintained at later times, we measured T cell proliferation based on CFSE dilution at 72 hours
194 post stimulation. Similar to what was observed for early activation markers, increasing substrate
195 stiffness produced graded increases in $CD4^+$ T cell proliferation, and the threshold dose required
196 to induce robust proliferation shifted as a function of substrate stiffness (Figure 4A,B). This effect
197 was particularly evident at low doses of pMHC-II (0.1-1ug/ml). Interestingly, although soft
198 hydrogels (2-4 kPa) elicited only very low levels of $CD4^+$ T cell proliferation, these substrates did
199 induce upregulation of CD25 in a high percentage of $CD4^+$ T cells, even in the undivided
200 populations (Figure 4C,D). This indicates that an activating signal was received, but was
201 insufficient to drive proliferation.

202 Since the threshold stimuli (stiffness and dose of pMHC-II) required to induce significant IL-2
203 production and proliferation were very similar (Figures 3C and 4B), we reasoned that the
204 threshold for proliferation might be driven by IL-2 availability. To test this, OT-II $CD4^+$ T cells were
205 stimulated on hydrogels with or without addition of 25 U/ml exogenous IL-2. Interestingly,
206 addition of IL-2 did not rescue the proliferation of T cells stimulated on soft surfaces (Figure 4E).
207 Thus, we conclude that in addition to influencing the signaling threshold for IL-2 production,
208 substrate stiffness also affects other IL-2 independent events needed for efficient T cell
209 proliferation.

210 Although early activation events in $CD8^+$ T cells did not exhibit stiffness sensitivity, we reasoned
211 that proliferative responses might behave differently. As shown in (Figure 5A,B), $CD8^+$ T cells
212 showed a mild stiffness-dependent proliferation response. The concentration of stimulatory

213 ligand needed to induce at least one round of division was similar across the entire stiffness range
214 Over successive rounds, increased stiffness did enhance the extent of proliferation, but the
215 differences were relatively small (Figure 5B). Interestingly, analysis of CFSE dilution as a function
216 of CD25 expression reveals evidence that $CD8^+$ T cells exhibit a binary stiffness response (Figure 5
217 C,D); at low doses of peptide ligand, cells stimulated on very stiff substrates (25kPa or plastic)
218 survived and proliferated, whereas cells stimulated on softer substrates were mostly lost (Figure
219 5C). From the standpoint of T cell priming, the significance of this observation is unclear, since
220 these stiffnesses are well outside the biologically relevant range we measured for DCs.

221 Taken together, our findings point to a mechanism in which stiffer substrates have a sensitizing
222 effect on $CD4^+$ T cells, similar to that of classical co-stimulatory molecules such as CD28 (Harding,
223 McArthur, Gross, Raulet, & Allison, 1992). When considered in this way, the relative lack of
224 stiffness responses in $CD8^+$ T cells fits with the fact that $CD8^+$ T cells are much less dependent on
225 costimulatory signals (McAdam, Schweitzer, & Sharpe, 1998).

226 **Degranulation of cytotoxic T cells shows mild stiffness sensitivity.**

227 Whereas naïve T cells are activated by DCs, effector T cells interact with many cell types. In
228 particular, cytotoxic $CD8^+$ T cells (CTLs) must respond to a variety of possible target cells, which
229 may differ widely with respect to stiffness. We therefore reasoned that CTL effectors might be
230 stiffness independent. To test this, *ex vivo* OTI $CD8^+$ T cells were activated on plastic surfaces and
231 grown in the presence of exogenous IL-2 to produce mature CTLs. To induce and detect release
232 of cytolytic granules, CTLs were re-stimulated on hydrogels coated with a range of pMHC-I
233 concentrations in the presence of fluorescent anti-CD107a antibody and analyzed by flow
234 cytometry. Degranulation showed only a mild stiffness dependency (Figure 5E), and stiffness
235 tended to affect the magnitude of degranulation rather than whether or not a degranulation
236 response was triggered. Interestingly, changes in substrate stiffness within the range of defined

237 for DCs (2-8kPa) had little or no impact on degranulation. Increased degranulation was only seen
238 on stiffer surfaces (12 and 25 kPa). This could have functional consequences for effector function
239 *in vivo*, since target cells in inflamed tissues can reach this stiffness range.

240 **Engagement the TCR complex by pMHC elicits the most prominent stiffness response**

241 Many current models for TCR mechanosensing are founded on the notion of TCR deformation
242 following engagement of cognate pMHC (Ma, Janmey, & Finkel, 2008). According to this concept,
243 forces applied by the T cell on the TCR-pMHC bond result in conformational changes within TCRαβ
244 (primarily the β chain), which are transmitted to intracellular components of the TCR/CD3
245 complex, leading to the initiation of downstream signaling (Das et al., 2015; Lee et al., 2015;
246 Swamy et al., 2016). Given this, we wondered whether engaging the TCR complex through the
247 CD3ε chain, as compared to direct TCRαβ engagement, would differentially affect T cell
248 mechanosensing. To test this, $CD4^+$ OT-II T cells were stimulated on hydrogels coated with anti-
249 CD3ε antibodies, anti-TCRβ antibodies, or pMHC-II monomers. T cell activation was measured at
250 72 hours based on proliferation (CFSE dilution) and expression of CD25 (Figure 6). All three ligands
251 induced a stiffness-dependent response for both proliferation and CD25 expression, but the
252 responses differed in significant ways. In general, stimulating T cells with pMHC-II resulted in the
253 strongest responses on the hydrogel surfaces; only on plastic surfaces did anti-CD3ε stimulation
254 yield a similarly strong response (Figure 6A,C). (Figure 6A). Importantly, on surfaces with a
255 stiffness similar to that of mature DCs (8kPa), stimulation with pMHC resulted in robust
256 proliferation, while stimulation with anti-CD3ε yielded a minimal response. On softer substrates
257 in the 2-4kPa range, pMHC elicited some proliferation, whereas stimulation with anti-CD3 did not.
258 Interestingly, stimulation with anti-TCRβ resulted in a mixed response. At high doses of antigen,
259 stimulation with anti-TCRβ yielded clear proliferative responses on substrates within the
260 biologically-relevant stiffness range. Analysis of CD25 expression patterns revealed a similar trend

261 (Figure 6D-F); on soft surfaces, pMHC yielded the strongest response, and anti-TCRβ was more
262 effective than anti-CD3ε. Taken together, these results indicate that T cells sense substrate
263 stiffness best through direct engagement of TCRαβ.

264 **The increased stiffness of mature DCs enhances their ability to prime T cells**

265 Our hydrogel assays show that T cell activation is enhanced by changes in stiffness over the range
266 observed for DC maturation, consistent with the idea that modulation of cortical stiffness is a
267 biophysical mechanism by which DCs control T cell activation. To test this directly, we sought
268 conditions under which we could manipulate the stiffness of mature DCs. We took advantage of
269 our finding that mature WASp knockout BMDCs are approximately 20% softer than WT controls
270 (Figure 2A; data are presented as absolute values in Figure 7A). WT and WASp$^{-/-}$ BMDCs were
271 pulsed with increasing concentrations of OVA$_{323-339}$ peptide and co-cultured with OT-II CD4^{+} T cells.
272 T cell proliferation was measured by CFSE dilution. As shown in Figure 7B, WASp$^{-/-}$ BMDCs did not
273 prime T cells as efficiently as WT BMDCs at low OVA concentrations. Higher concentrations of
274 OVA rescued this defect, showing that loss of WASp shifts the dose of peptide needed rather than
275 affecting T cell priming *per se,* in keeping with the view that DC stiffness provides a costimulatory
276 signal. We next attempted to test T cell priming activity of DCs that are stiffer than WT cells. We
277 tested several genetic manipulations, most of which did not significantly increase the cortical
278 stiffness of mature BMDCs. We did find that overexpression of a constitutively active form of
279 WASp (I294T, CA-WASp (Beel et al., 2009)) increased cortical stiffness of mature BMDCs by
280 approximately 20% relative to WT cells (Figure 7A), but these BMDCs failed to prime T cells more
281 efficiently (Figure 7C). Expression of CA-WASp only enhances BMDC stiffness to approximately
282 5kPa, and based on our hydrogel studies, this increase is unlikely to be sufficient to enhance T cell
283 activation. It seems likely that conditions that stiffen DCs to 10kPa or more would further enhance
284 T cell responses, but we were unable to test this directly, and it is not clear whether this happens

285 in vivo. Nonetheless, the studies using WASp-/- DCs show that changes in DC stiffness within the
286 range observed during maturation has a significant impact on their ability to efficiently prime a T
287 cell response.

288 **DISCUSSION**

289 Recent work from several labs clearly shows that T cell activation involves mechanical cues. We
290 have previously shown that the DC cytoskeleton constrains the mobility of stimulatory ligands
291 on the DC surface, enhancing T cell activation by opposing the forces exerted by the T cell on the
292 corresponding receptors (Comrie et al., 2015). In the current study, we elucidate a second
293 mechanism whereby the DC cytoskeleton enhances T cell activation. We show that actin
294 remodeling during DC maturation increases the cortical stiffness of DCs by 2-3 fold, and that T
295 cell activation is enhanced by increases in stiffness over the same range. Importantly, increased
296 stiffness lowers the threshold dose of TCR ligand needed for T cell activation, as expected if
297 substrate stiffness serves as a costimulatory signal. In keeping with this concept, $CD4^+$ T cells
298 showed more profound stiffness-sensitivity than $CD8^+$ T cells, especially at early times in the
299 activation process. Together, these results indicate that stiffening of the DC cortex during
300 maturation provides biophysical cues that work together with canonical costimulatory cues to
301 enhance T cell priming.

302 Modulation of actin architecture has long been appreciated as an essential feature of DC
303 maturation. Changes in the DC actin cytoskeleton facilitate the transition from highly endocytic
304 tissue-resident cells to migratory cells specialized for antigen presentation (Burns et al., 2004;
305 Burns et al., 2001). Our findings reveal a new facet of this process. We show that immature DCs
306 are very soft, and that upon maturation, their cortical stiffness is increased by 2-3 fold. This is
307 true for cultured BMDCs treated with LPS *in vitro*, as well and splenic DCs harvested from LPS-

308 treated mice. A similar trend was reported by Bufi et al for human monocyte-derived DCs (Bufi
309 et al., 2015), although that study reported lower absolute Young's modulus values. While we
310 used AFM indentation, Bufi et al. used microplate rheology. Since different methods for
311 measuring cell mechanical properties produce absolute Young's modulus values that can vary by
312 as much as 100 fold (Wu et al., 2018), it seems likely that the apparent discrepancy in absolute
313 values stems from technical differences between the two studies. Nevertheless, it is clear from
314 both studies that the stiffness of the DC cortex is modulated during maturation.
315
316 The observed increase in stiffness depends on changes in actin architecture; whereas
317 depolymerization of actin filaments has no effect on the stiffness of immature DCs, the increase
318 associated with maturation depends on intact filaments, and is sensitive to inhibitors of actin
319 polymerizing molecules. While it remains to be determined exactly which actin regulatory
320 pathways control cortical stiffness in mature DCs, our data show that both Arp2/3 complex and
321 formins are involved. Moreover, we find that DCs lacking the Arp2/3 activator WASp are
322 abnormally soft. In keeping with these findings, DC maturation is known to induce changes in
323 the activation state and localization of Rho family GTPases, especially Cdc42, a molecule that
324 can activate both WASp and formins (Garrett et al., 2000; Vargas et al., 2016; West et al., 2000).
325 Since the overall levels of active Cdc42 are diminished during DC activation, it seems likely that
326 the observed increase in cortical stiffness results from redistribution of the active pool.

327 We show that DC cortical stiffness is a cell-intrinsic property that is unaffected by substrate
328 stiffness. In this respect, DCs are different from other cell types that adapt their stiffness to
329 differences in substrate compliance (Byfield et al., 2009; Tee et al., 2011). The ability of DCs to
330 maintain constant stiffness despite changing environmental cues is reminiscent of previous work
331 showing that DCs rapidly change their method of locomotion in order to maintain consistent

332 migration speed and shape while crossing over different surfaces (Renkawitz et al., 2009). This
333 behavior has been proposed to allow DCs to pass through tissues with widely different
334 mechanical properties. In the same way, we propose that the ability of DCs to regulate cortical
335 stiffness as a function of maturation state in spite of environmental cues reflects the importance
336 of this property for priming an appropriate T cell response.

337 A central finding of this paper is that changes in DC stiffness serves as a costimulatory signal for
338 T cell priming. By using a matrix of different hydrogels spanning the biologically relevant range
339 defined for immature and mature DCs (2 – 8 kPa), coated with increasing pMHC concentrations,
340 we found that stimulatory substrates with lower stiffness required higher concentrations of
341 pMHC to achieve T cell activation. Similarly, when compared to WT DCs, softer WASp knockout
342 DCs required higher concentrations of OVA peptide to induce the same level of proliferation.
343 Our results indicate that increases in cortical stiffness, together with diminished ligand mobility
344 (Comrie et al., 2015), represent biophysical cues that are modulated in parallel with
345 upregulation of costimulatory ligands and cytokines as a fundamental part of DC maturation.
346 When interacting T cells engage pMHC complexes and costimulatory ligands on the DC surface,
347 they integrate this biophysical input along with other canonical costimulatory signals.

348 In addition to lowering the antigenic threshold for T cell activation, changes in stiffness may
349 present a new signaling mechanism by which DCs control T cell fate and differentiation. Bufi et
350 al. showed previously that human monocyte-derived DCs responding to different maturation
351 signals vary in their stiffness (Bufi et al., 2015). Interestingly, they found that treatment with the
352 tolerizing cytokines TNFα and prostaglandin E2 results in DCs that are even softer than
353 immature cells. Tolerogenic DCs exhibiting partially immature phenotypes have been shown to
354 induce differentiation of regulatory T cells (Doan, McNally, Thomas, & Steptoe, 2009; Gleisner,
355 Rosemblatt, Fierro, & Bono, 2011; Gordon, Ma, Churchman, Gordon, & Dawicki, 2014). This

356 effect is usually attributed to low expression of T cell ligands or cytokines, but based on our
357 data, we propose that biophysical properties of the DC cortex also play a role. Going forwards, it
358 will be important to ask how DC stiffness is modulated in response to different environmental
359 cues, and whether this further shapes T cell responses.

360 While we demonstrate T cell stiffness responses on soft surfaces emulating DCs, others have
361 reported T cell stiffness responses on very stiff surfaces (Judokusumo et al., 2012; O'Connor et
362 al., 2012). We found that very stiff substrates (25kPa hydrogels and plastic surfaces in the GPa
363 range) elicit strong responses. This was true for proliferation, IL-2 secretion and degranulation.
364 Similarly, recent analysis of human $CD4^+$ effector T cells shows that re-stimulation on soft
365 surfaces induces upregulation of genes related to cytokine signaling and proliferation, while
366 restimulation on very stiff surfaces (100 kPa) triggers expression of an additional genetic
367 program that includes metabolic proteins related to glycolysis and respiratory electron transport
368 (Saitakis et al., 2017). The physiological relevance of these augmented responses is unclear,
369 since T cells probably never encounter such stiff stimulatory surfaces *in vivo*. Nonetheless, such
370 findings raise important questions about traditional *in vitro* assays of T cell function, which often
371 utilize glass or plastic stimulatory surfaces.

372 The observation that T cells respond to APC stiffness is best understood in the context of
373 evidence that T cells exert force on an interacting APC through the TCR complex (Bashour et al.,
374 2014; Blumenthal & Burkhardt, 2020; Hui et al., 2015; Husson et al., 2011; Li et al., 2010;
375 Sawicka et al., 2017), with the amount of force corresponding to APC stiffness (Husson et al.,
376 2011; Sawicka et al., 2017). Apart from being a requirement for activation (Li et al., 2010;
377 Pryshchep et al., 2014), force transduction has been shown to promote peptide discrimination
378 by influencing bond lifetimes (Das et al., 2015; Liu et al., 2014). Importantly, it appears that the
379 TCR's ability to sense stiffness is closely related to its ability to transduce force-dependent

380 signals during T cell-APC interaction. Indeed, there is evidence that signaling downstream of TCR
381 engagement is increased on stiffer substrates (Judokusumo et al., 2012) and that the location of
382 early tyrosine phosphorylation events corresponds to sites of maximum traction force (Bashour
383 et al., 2014). We propose that stiffer substrates allow T cells to exert more force through TCR
384 interactions, and consequently induce more effective signaling. This accounts for the co-
385 stimulatory property of substrate stiffness on T cell activation.

386 The mechanism by which force application on the TCR is translated into biochemical signals
387 remains controversial. Nevertheless, there is evidence to suggest that force applied on the TCR
388 complex induces conformational changes within TCRαβ that exposes ITAM sites on the CD3 and
389 TCRζ chains for phosphorylation and downstream signaling [57,58]. Importantly, conformational
390 changes are mainly attributed to extension of the CβFG loop region within TCRβ (Das et al.,
391 2015), which serves as a lever to push down on the CD3 complex (Sun, Kim, Wagner, & Reinherz,
392 2001), exposing ITAM sites (Xu et al., 2008). In support of this idea, we found that the way in
393 which the TCR is engaged influences T cell stiffness sensing. Within the biologically relevant
394 stiffness range (2-8 kPa), T cells were activated only when TCRαβ was engaged directly; indirect
395 engagement through anti-CD3 resulted in almost no response. We postulate that direct TCRαβ
396 engagement leads to conformational changes that are transmitted appropriately for efficient
397 initiation of downstream signaling, whereas engagement of CD3 induces smaller changes and
398 more limiting downstream signaling. This effect may be most evident on soft substrates,
399 because force-dependent signaling is limiting in this setting. We note that on these soft
400 substrates, pMHC induced stronger T cell activation than anti-TCRβ. This may reflect the
401 involvement of CD4 in the former, which leads to more efficient recruitment of Lck to the TCR
402 complex.

403 Although our focus here is on the role of stiffness sensing in priming of naïve T cells, we find that
404 effector $CD8^+$ T cells also exhibit stiffness-dependent degranulation responses. Similarly, Saitakis
405 et al. have shown that restimulating $CD4^+$ effector T cells on surfaces of different stiffness
406 induces differential gene expression and cytokine production (Saitakis et al., 2017). Since DCs
407 increase their cortical stiffness during maturation, a stiffness dependent mechanism for naïve T
408 cell priming makes biological sense. Effector T cells, however, interact with a variety of APCs. In
409 particular, cytotoxic $CD8^+$ T cells are expected to kill any infected cell throughout the body with
410 no stiffness bias. The physiological significance of stiffness sensitivity for effector T cells remains
411 unclear. One intriguing possibility is that mechanosensing is an obligate component of the
412 feedback loop that underlies force-dependent TCR triggering.

413 The IS is often described as a platform for information exchange between the T cell and APC.
414 Together with our recent work on ligand mobility, the findings presented here indicate that the
415 mechanical properties of the APC side of the IS influence T cell priming, likely because they
416 augment force-dependent conformational changes in TCRs, integrins, and potentially other
417 molecules. Going forward, it will be important to determine how these properties are
418 modulated during DC maturation, and whether there are also local changes induced by signaling
419 events taking place at the IS. In addition, it will be important to tease apart the molecular events
420 through which T cells sense and respond to these mechanical cues.

421 **MATERIALS AND METHODS**

422 **Key Resource Table**

Reagent type (species) or resource	Designation	Source or reference	Identifiers	Additional information
antibody	APC/APC-Cy7 anti-CD4 (rat, clone GK1.5)	Biolegend	Biolegend:100411/10041; RRID:100411/AB_312698	Flow (1:350)
antibody	APC/PE-Cy7 anti-CD8 a (rat, clone 53-6.7)	Biolegend	Biolegend: 00711/100721; RRID:AB_312750/AB_312760	Flow (1:350)
antibody	anti-CD3ε (A. hamster, clone 145-2C11)	BioXCell	BioXcell: BE0001-1; RRID: AB_1107634	0.003 µg/mL - 10 µg/mL
antibody	anti-CD3ε (Armenian hamster, clone PV1)	BioXCell	BioXcell:BE0015-5; RRID:AB_1107628	1 µg/mL - 2 µg/mL
antibody	Anti-CD86 (rat, clone GL-1)	BioXCell	BioXcell: BE0025; RRID: AB_1107678	Stain (1:100)
antibody	APC-Cy7 anti-CD86 (rat, clone GL-1)	BioLegend	BioLegend:105029; RRID:AB_2074993	Flow (1:100)
antibody	PE anti-MHC-II (rat, clone M5/114.15.2)	BioLegend	BioLegend:107607; RRID:AB_313322	Flow (1:100)
antibody	APC anti-CD11c (rat, clone N418)	BioLegend	BioLegend:117309; RRID:AB_313778	Flow (1:100)
antibody	PE-antiCD107a (LAMP-1) (rat, clone 1D4B)	BioLegend	BioLegend:121611; RRID:AB_1732051	2 µg/mL
chemical compound, drug	Cytochalasin-D	EMD Millipore	EMD Millipore: 250255; CAS:22144-77-0	10 µM
chemical compound, drug	Latrunculin-B	EMD Millipore	EMD Millipore: 428020; CAS:76343-94-7	10 µM
chemical compound, drug	(S)-nitro-Blebbistatin	Cayman Chemical	Cayman Chemical:13891; CAS:856925-75-2	50 µM
chemical compound, drug	CK666	EMD Millipore	Millipore: 182515; CAS:442633-00-3	100 µM
chemical compound, drug	Y27632	SIGMA	SIGMA:688000; CAS:146986-50-7	25 µM
chemical compound, drug	SMIFH2	SIGMA	SIGMA:344092; CAS:340316-62-3	10 µM

chemical compound, drug	Escherichia coli 026:B6; LPS	SIGMA	SIGMA:L2762; ECN:297-473-0	200 ng/mL
chemical compound, drug	Collagenase D	SIGMA	SIGMA: COLLD-RO; EC#:3.4.25.3	2 mg/mL
chemical compound, drug	IL-2	NIAID, NIH	N/A	25U;100U
chemical compound, drug	streptavidin-coated polystyrene beads	Spherotech	Spherotech: SVP-60-5	
chemical compound, drug	EZ-link NHS biotin kit	Thermo Fisher Scientific	Thermo Fisher Scientific: 21217	
chemical compound, drug	CFSE	Invitrogen	Invitrogen: C34570	
commercial assay or kit	CF555 Mix-n-Stain	Biotium	Biotium:92234	
commercial assay or kit	MACS pan-dendritic cell isolation kit	Miltenyi Biotec	Miltenyi: 130-100-875	
commercial assay or kit	mouse IL-2 ELISA kit	Invitrogen	Invitrogen: 88-7024-88	
gene (mouse)	*Was*; Wiskott–Aldrich syndrome gene	DOI:10.1084/jem.20091245	MGI:105059; NCBI Gene: 22376	
other	Hydrogel surfaces (96 well plates)	Matrigen	EasyCoat Softwell 96G	Customized plates
other	AFM 1 µM spherical polystyrene probe	Novascan	Novascan: PT.PS	Si_3N_4 cantilever k=0.06 N/m
peptide, recombinant protein	Peptide MHC-II Complex	NIH Tetramer Core	I-A^b	Sequence: HAAHAEINEA
peptide, recombinant protein	Ovalbumin 323–339; $OVA_{323–339}$	Anaspec	Anaspec: AS-27025; LOT:1755317	Sequence: ISQAVHAAHAEINEAGR
recombinant DNA reagent	pLX301 (plasmid)	Addgene	Addgene: 25895; RRID: Addgene_25895	DOI:10.1038/nmeth.1638
software, algorithm	FlowJo	FlowJo LLC	RRID:SCR_008520	
software, algorithm	NanoScope Analysis	Broker	N/A	
strain, strain background (Mice)	OT-II Transgenic mice / OT-II	Jackson Laboratories	Stock: 004194; RRID:IMSR_JAX:004194	B6.Cg-Tg(TcraTcrb)425Cbn/J

strain, strain background (Mice)	OT-I Transgenic mice / OT-I	Jackson Laboratories	Stock: 003831; RRID:IMSR_JAX:003831	C57BL/6-Tg(TcraTcrb)1100Mjb/J
strain, strain background (Mice)	*Was*$^{-/-}$; WASP-,WASp-KO	Jackson Laboratories	Stock: 003292; RRID: IMSR_JAX:003292	129S6/SvEvTac-Was^{tm1Sbs}/J
strain, strain background (Mice)	*Hlcsp1*$^{-/-}$; HS1-KO	David Rawlings, MD.	PMCID: PMC394441	
strain, strain background (Mice)	*Fcsn1-/-*	KOMP Repository, UC Davis	MGI:5605764	Fscn1$^{tm1.1(KOMP)Vlcg}$

423

424 **Inhibitors and antibodies**

425 Cytochalasin-D and Latrunculin-B were from EMD Millipore, (S)-nitro-Blebbistatin was from
426 Cayman Chemical, CK666 was from Calbiochem, and Y27632 and SMIFH2 were from Sigma-
427 Aldrich. Flow cytometry antibodies: rat anti-CD4 APC/APC-Cy7 (clone RM4-5), rat anti-CD8a
428 APC/PE-Cy7 (clone 53-6.7), Armenian hamster anti-CD69 APC (clone H1.2F3) and rat anti-CD25 PE
429 (clone PC61) were all from BioLegend. Surface coating antibodies: Armenian hamster anti-CD3ε
430 (clone 2C11), and Armenian hamster anti-CD28 (Clone PV1) were from BioXCell. Biotinylated
431 Armenian hamster anti-CD3ε (clone 2C11) was from Invitrogen, and biotinylated mouse anti-
432 TCRVβ5.1/5.2 (clone MR9-4) was from BD Bioscience. Dendritic cell staining: anti-CD86 CF555 was
433 made by conjugating purified rat anti-CD86 (BioXCell) with CF555 conjugated dye from Biotium as
434 per the manufacturer's protocol.

435 **Mice**

436 All mice were originally obtained from The Jackson Laboratory and housed in the Children's
437 Hospital of Philadelphia animal facility, according to guidelines put forth by the Institutional
438 Animal Care and Use Committee. C57BL/6 mice (WT) were purchased from Jackson Labs. HS1-
439 KO mice on the C57BL/6 background have been previously described(Taniuchi et al., 1995) and
440 were a kind gift from doctor David Rawlings at the University of Washington. *Was*$^{-/-}$ mice were

441 purchased from Jackson labs (Snapper et al., 1998) and fully backcrossed to a C57BL/6
442 background. All mouse strains were used as a source of bone marrow from which to generate
443 BMDCs. Mice bearing a gene trap mutation in the Fscn1 gene (Fscn1$^{tm1(KOMP)Vlcg}$), which abrogates
444 expression of the protein Fascin 1, were generated by the KOMP Repository at UC Davis, using
445 C57BL/6 embryonic stem cells generated by the Texas A&M Institute for Genomic Medicine.
446 Because these mice proved to have an embryonic lethal phenotype, fetal liver chimeras were used
447 as a source of bone marrow precursors. Heterozygous mating was performed, and fetal livers
448 were collected after 15 days of gestation and processed into a single-cell suspension by mashing
449 through a 35-µm filter. Embryos were genotyped at the time of harvest. Cells were resuspended
450 in freezing media (90% FCS, 10% DMSO) and kept at −80 °C until used. Thawed cells were washed,
451 counted, resuspended in sterile PBS and injected i.v. into sub-lethally irradiated 6-week-old
452 C57BL/6 recipients, 1×10^6 cells per mouse. Chimeras were used as a source for fascin KO bone
453 marrow ~6 weeks after transfer. OT-I T cells were prepared from heterozygous OT-I TCR Tg mice,
454 which express a TCR specific for ovalbumin 257-264 (amino acid sequence SIINFEKL) presented
455 on H-2K^b (Hogquist et al., 1994). OT-II T cells were prepared from heterozygous OT-II TCR Tg mice,
456 which express a TCR specific for ovalbumin 323–339 (amino acid sequence
457 ISQAVHAAHAEINEAGR) presented on I-A^b (Barnden, Allison, Heath, & Carbone, 1998).

458 **Cell culture**

459 Unless otherwise specified, all tissue culture reagents were from Invitrogen/Life Technologies.
460 GM-CSF was produced from the B78H1/GMCSF.1 cell line (Levitsky et al., 1996). HEK-293T cells
461 (ATCC) were cultured in DMEM supplemented with 10% FBS, 25mM Hepes,
462 penicillin/streptomycin, GlutaMAX, and non-essential amino acids.

463 Generation of bone marrow derived dendritic cells (BMDCs) was similar to (Inaba et al., 1992).
464 Briefly, mouse long bones were flushed with cold PBS, the resulting cell solution was passed

465 through a 40 µm strainer, and red blood cells were lysed by ACK lysis. Cells were washed once
466 with RPMI-1640 and then either frozen for later use in RPMI-1640 containing 20% FBS, 10%
467 DMSO, or plated in 10 cm bacterial plates in BMDC culture media (RPMI-1640, 10% FBS,
468 penicillin/streptomycin, GlutaMax and 1% GM-CSF supernatant). On day 3 of culture, dishes were
469 supplemented with 10 ml of BMDC culture media. On Day 6, 10 ml of media were replaced, by
470 carefully collecting media from the top of the dish and slowly adding fresh media. BMDC
471 differentiation was verified by flow cytometry, showing 80-90% CD11c positive cells. BMDC
472 maturation was induced on days 7 or 8; immature BMDCs were harvested and re-plated in a 6cm
473 tissue culture dish in 5 ml of BMDC media supplemented with 200 ng/ml LPS (*Escherichia coli*
474 026:B6; Sigma-Aldrich) for at least 24h. Maturation was verified by flow cytometry, with mature
475 BMDCs defined as Live/CD11c^{+}/CD86^{high}/MHC-II^{High} cells. To generate splenic DCs, spleens from
476 C57BL/6 mice were cut to smaller pieces and digested with Collagenase D (2 mg/ml, Sigma) for 30
477 min at 37°C, 5%CO_2. Cells were washed and labeled for separation by negative selection using a
478 MACS pan-dendritic cell isolation kit (Miltenyi Biotec).

479 Primary mouse T cells were purified from lymph nodes and spleens using MACS negative selection
480 T cell isolation kits (Miltenyi Biotec). In the case of CD4^{+} T cells, ex vivo cells were used, as isolation
481 yielded high fractions of naïve cells. In the case of CD8^{+} T cells, naïve T cells were isolated, as ~45%
482 of T cells isolated from OT-I mice showed some level of activation. To generate cytotoxic CD8^{+} T
483 cells (CTLs), purified murine CD8^{+} cells were activated on 24-well plates coated with anti-CD3ε
484 and anti-CD28 (2C11 and PV1, 10µg/ml and 2 µg/ml respectively) at 1x10^{6} cells per well. After
485 24h, cells were removed from activation and mixed at a 1:1 volume ratio with complete T cell
486 media (DMEM supplemented with penicillin/streptomycin, 10% FBS, 55µM β-mercaptoethanol
487 GlutaMAX, and non-essential amino acids), containing recombinant IL-2 (obtained through the
488 NIH AIDS Reagent Program, Division of AIDS, NIAID, NIH from Dr. Maurice Gately, Hoffmann - La

489 Roche Inc (Lahm & Stein, 1985)), to give a final IL-2 concentration of 100 units/ml. Cells were
490 cultured at 37°C and 10% CO_2, and passaged as needed to be kept at $0.8x10^6$ cells/ml for 7 more
491 days. CTLs were used at days 8 or 9 after activation.

492 **Plasmid construction, viral production, and transduction of DCs:**

493 A constitutively active form of WASp (CA-WASp) was engineered by subcloning WASp cDNA into
494 a pLX301 vector (Addgene), introducing an I294T point mutation (Westerberg et al., 2010) by site-
495 directed mutagenesis, and confirming by sequencing. To generate recombinant lentivirus, HEK-
496 293T cells were co-transfected using the calcium phosphate method with psPAX2 and pMD2.G,
497 together with the DNA of interest in pLX301. For transduction, BMDCs were plated in untreated
498 6 well plates at $2x10^6$ cells/well in 3 ml of BMDC media. BMDC transduction was carried out on
499 day 2 of culture; lentiviral supernatants were harvested from HEK-293T cells 40hr post
500 transfection, supplemented with 8 µg/ml Polybrene (Sigma-Aldrich), and used immediately to
501 transduce BMDCs by spin-infection at 1000xG, 37°C for 2hr. After resting the cells for 30 min at
502 37°C, 5% CO_2, lentivirus-containing media was replaced with normal BMDC culture media. On day
503 5 of culture, puromycin (Sigma-Aldrich) was added to a final concentration of 2 µg/ml to allow
504 selection of transduced BMDCs. Maturation of transduced cells was induced on day 8 by adding
505 200 ng/ml of LPS in puromycin-free media.

506 **Flow Cytometry**

507 All cells were stained with Live/Dead aqua (ThermoFisher) following labeling with appropriate
508 antibodies in FACS buffer (PBS, 5% FBS, 0.02% NaN_3, and 1 mM EDTA). Flow cytometry was
509 performed using either the Cytoflex LX or CytoFlex S cytometer (Beckman Coulter) and analyzed
510 using FlowJo software (FlowJo LLC). T cells were gated based on size, live cells, and expression of
511 CD4 or CD8 (depending on the experiment). DCs were incubated for 10 min on ice with the Fc

512 blocking antibody 2.4G2 prior to staining. DCs were gated based on size, live cells, and CD11c
513 expression. Mature DCs were further gated based on high expression of MHC-II, CD86 or CD80.

514 **T cell activation on stimulatory gel surfaces**

515 96 well plates coated with polyacrylamide hydrogels spanning a stiffness range of 2 – 25 kPa were
516 obtained from Matrigen. Hydrogel stiffness was verified by AFM at different locations around the
517 hydrogel surface (Figure 3 - Figure Supplement 1). Surfaces were first coated with 10 µg/ml of
518 NutrAvidin (ThermoFisher) and 2 µg/ml anti-CD28 (clone PV1) overnight at 4°C. Primary amines
519 in the NutrAvidin form covalent bonds with quinone functional groups within the hydrogels. The
520 gel pore size is on the order of tens of nanometers, such that cells can only interact with ligands
521 bound on the gel surface. Surfaces were then washed twice with 200 µL of PBS and coated with
522 varying concentrations of biotinylated pMHC monomers (NIH tetramer core facility) for 2 hours
523 at 37°C. Where antibodies were used for coating, surfaces were coated with varying
524 concentrations of either biotinylated anti-CD3ε (clone 2C11), or biotinylated anti-TCRvβ5.1/5.2
525 (clone MR9-4). Surfaces were than washed 2 times with 200 µL of PBS, and blocked for 10 min
526 with T cell media containing 10% FBS prior to addition of $2.0x10^5$ cells/well. Control studies
527 showed that stimulatory ligands bound slightly less well to stiffer hydrogel surfaces (Figure 3 -
528 Figure Supplement 2). Stiffer surfaces show the same or higher activating properties across all
529 assays, ruling out the possibility that differences in T cell activation are due to differential ligand
530 binding. Importantly, initial experiments included a 1 kPa hydrogel surface that yielded no
531 response across all assays. Therefore, data from this condition is not shown and was not included
532 in repeated experiments. For experiments where exogenous IL-2 was added, media was
533 supplemented with IL-2 to a final concentration of 25 U/ml. To measure IL-2 secretion,
534 supernatants were harvested 22-24 hours post stimulation, and IL-2 concentration was measured
535 using a mouse IL-2 ELISA kit (Invitrogen). For early activation marker expression assays, cells were

536 plated immediately after isolation, and harvested 22-24 hours post stimulation for flow cytometry
537 analysis. For CFSE dilution assays, purified cells were washed once with PBS and stained for 3 min
538 with 2.5 µM CFSE (ThermoFisher). After quenching the excess CFSE by addition of 1 ml FBS for 30
539 seconds, cells were washed and plated. Cells were harvested 68-72 hours post stimulation for
540 flow cytometry analysis. For ligand comparison assays, surfaces were first coated with 10 µg/ml
541 of NutrAvidin (ThermoFisher) and 2 µg/ml anti-CD28 (PV1) overnight at 4°C. Surfaces were then
542 washed twice with 200 µL of PBS and coated with varying concentrations of biotinylated ligands
543 (anti-TCRVβ5.1/5.2, anti-CD3ε, or pMHC-II monomers) for 2 hours at 37°C.

544 **Cytotoxic T cell degranulation assays**

545 Assays were conducted on day 8 or 9 of culture. $2x10^5$ CTLs were plated onto surfaces coated with
546 various concentrations of pMHC-I in the presence of 2 µg/ml PE-conjugated anti-CD107a. After 3
547 hours of re-stimulation, CD107a labeling was quantified by flow cytometry analysis. Cells were
548 gated based on size, live cells, and expression of $CD8^+$. CD107a mean fluorescence intensity (MFI)
549 was extracted using FlowJo.

550 **T cell priming assays**

551 Priming assays were carried out in round bottom 96 well plates. $5x10^4$ LPS-matured BMDCs were
552 plated in each well and pulsed with $OVA_{323–339}$ peptide at various concentrations (0.1 – 1 µg/ml).
553 $1.5x10^5$ CFSE stained, OT-II $CD4^+$ T cells were added to each well and incubated for 68-72 hours.
554 Cells were then harvested and analyzed using flow cytometry.

555 **Atomic force microscopy (AFM)**

556 All experiments were carried out at room temperature using a Bruker Bioscope Catalyst AFM
557 mounted on a Nikon TE200 inverted microscope. Micro-indentation measurements were made
558 with a spherical tip from Novascan. The tip was comprised of a 1 µm silicon dioxide particle

559 mounted on a silicon nitride cantilever with a nominal spring constant of 0.06 N/m; each
560 cantilever was calibrated using the thermal fluctuation method. The AFM was operated in fluid
561 contact mode, with 2 Hz acquisition. Total vertical cantilever displacement was set to 5 µm,
562 producing a maximal approach/retraction speed of ~20 µm/sec. Maximal deflection (Trigger
563 threshold) was adjusted for each cantilever to apply a maximal force of 6 nN on the measured cell
564 (e.g. for a 0.06 N/m cantilever, the trigger threshold was set to 100 nm). The actual indentation
565 depth was ~1.5 µm depending on the measured cell stiffness (Figure 1 – Supplement Figure 2).
566 Analysis of force-distance curves was carried out using the Nanoscope Analysis software (Bruker).
567 The Young's modulus was extracted using the Hertzian model for spherical tips with a contact
568 point-based fitting on the extend curve data. For each individual cell, two separate measurements
569 were conducted at different locations near, but not directly over the nucleus. The reported cell
570 stiffness value represents the average between these independent measurements. Note that
571 when measurements of cortical stiffness were made over the nucleus, no significant differences
572 in Young's modulus values were found (not shown). To measure BMDC stiffness, $1x10^5$ cells
573 (untreated or LPS matured) were seeded onto Poly L-lysine coated coverslips and allowed to
574 spread for 4 hours at 37°C, 5% CO_2. Prior to data acquisition, cells were incubated for 10 min with
575 the Fc blocking antibody 2.4G2, washed and stained for CD86 for 20 min, then washed and
576 mounted on the AFM. All antibody incubations and data acquisition steps were performed in L-
577 15 media (Gibco) supplemented with 2mg/ml glucose. For treated cell measurements, drugs
578 [Latrunculin-B (10 µM), Cytochalasin-D (10 µM), s-nitro-Blebbistatin (50 µM), Y27632 (25 µM),
579 CK666 (100 µM), or SMIFH2 (10 µM)] were pre-incubated with the cells at 37°C, 5% CO_2 for 30 min
580 prior to Fc blocking and maintained in the cultures throughout staining and data acquisition.

581 **Statistical Methods**

582 All datasets were subjected to outlier analysis prior to execution of statistical testing. Outliers
583 were defined as data points with values outside the range of mean +/- 2.5xStDev, and were
584 deleted from the dataset. Testing for a statistically significant difference between experimental
585 groups was done using an unpaired one-way ANOVA test with a post-hoc Tukey correction for
586 multiple comparisons.

587 Throughout the paper, data shown represents biological, and not technical, replicates. For
588 BMDC assays, a single experiment constitutes measurement of multiple cells from a fresh DC
589 culture, starting from frozen or freshly harvested bone marrow. For splenic DCs, a single
590 experiment constitutes measurement of multiple cells freshly purified from the spleen of a
591 single mouse. In each experiment, WT or untreated cells were measured side by side with
592 treated cells as a standard control. For T cell assays, a single experiment constitutes cells freshly
593 purified from spleen and lymph nodes of a single animal. All CFSE dilution assays were executed
594 in technical duplicates, although a single data set is presented. When needed, figure legends
595 describe the quantity of technical repeats used in an experiment.

596 **ACKNOWLEDGEMENTS**

597 The authors thank Florin Tuluc and Jennifer Murray from the Children's Hospital of Philadelphia
598 Flow Cytometry core. We thank the biomechanics core of the Institute of Translational Medicine
599 and Therapeutics (ITMAT) at the University of Pennsylvania for use of the Atomic Force
600 Microscope and the NIH tetramer core facility for provision of MHC-peptide complexes. We thank
601 Dr. Shuixing Li and Dr. Nathan Roy for expert technical assistance, Dr. Nathan Roy and Mr. Tanner
602 Robertson for critical reading of the manuscript, and members of the Burkhardt laboratory for
603 many helpful discussions. This work was supported by NIH grants R01 GM104867 and R21
604 AI32828 to JKB.

605 **ETHICS STATMENT**

606 All studies, breeding and maintenance of animals was performed under Animal Care and Use
607 Protocol #667, as approved by The Children's Hospital of Philadelphia Institutional Animal Care
608 and Use Committee.

609 **FIGURE LEGENDS**

610 **Figure 1. DC maturation induces an actin-dependent increase in cortical stiffness.**

611 (A) BMDCs were untreated or matured by treatment with LPS, and cortical stiffness was
612 measured by AFM micro-indentation. Fluorescent anti-CD86 labeling was used to select
613 immature (CD86-negative) or mature (CD86 high) cells. (B) E*x-vivo* DCs were purified from
614 spleens of untreated mice or from mice injected with LPS 24 hours prior to harvesting the
615 spleen, and analyzed as in A. (C) Immature or LPS matured BMDCs either left untreated or
616 treated with 10µm of the actin de-polymerizing agents Latrunculin-B or Cytochalasin-D prior to
617 AFM measurements. (D) Immature or LPS matured BMDCs were plated on substrates of
618 different stiffness prior to AFM measurements. Data are pooled from 2-3 independent
619 experiments. Each data point represents an average of two stiffness measurements at different
620 locations around a single cell nucleus. Error bars denote standard deviation. n.s non-significant,
621 **$p<0.01$, ****$p<0.0001$ calculated by an unpaired one-way ANOVA, post-hoc Tukey corrected
622 test.

623 **Figure 2. Effects of actin regulatory proteins on DC cortical stiffness.**

624 Murine BMDCs from WT mice or mice lacking key actin-associated proteins were untreated or
625 matured by treatment with LPS, and cortical stiffness was measured by AFM micro-indentation.
626 To facilitate comparison between experiments, results were normalized to values of mature WT
627 BMDCs in each experiment. (A) Cortical stiffness of BMDCs from mice lacking important actin
628 modulating proteins. (B) Cortical stiffness of WT BMDCs treated with cytoskeletal inhibitors.
629 CK666 (100 µM) was used to inhibit branched actin polymerization by Arp2/3. SMIFH2 (10 µm)
630 was used to inhibit linear actin polymerization by formins. Acto-myosin contractility was
631 inhibited directly with Blebbstatin (50 µM) or indirectly with the Rho-kinase inhibitor Y27623 (25
632 µM). All drugs had no effect on immature BMDCs (data not shown). Data points for untreated

633 WT BMDCs (both immature and mature) were pooled from all experiments as a reference. The
634 dashed line represents the average stiffness of untreated mature WT BMDCs from all
635 experiments. Data are pooled from 2-3 independent experiments. Each data point represents an
636 average of two stiffness measurements at different locations around a single cell nucleus. Error
637 bars denote standard deviation. n.s non-significant, *p<0.05, **p<0.01, ***p<0.001,
638 ****p<0.0001 calculated by an unpaired one-way ANOVA, with post-hoc Tukey correction.

639 **Figure 3. $CD4^+$ and $CD8^+$ T cells demonstrate vastly different stiffness responses.**
640 Murine T cells were purified from lymph nodes and spleen and activated on stimulatory
641 acrylamide hydrogel surfaces with a stiffness range of 2 – 25 kPa (and plastic). Stimulatory
642 surfaces were coated with the indicated concentrations of pMHC-I or pMHC-II together with 2
643 µg/ml anti-CD28 to stimulate OT-I $CD8^+$ or OTI-II $CD4^+$ T cells, respectively. (A,B,D,E) Cells were
644 harvested 24 hours post activation and expression of early activation markers was measured by
645 flow cytometry. Data represent averages +/- SEM of percent positive cells from N=3
646 independent experiments. (A,B) $CD4^+$ T cells show profound stiffness dependent expression of
647 both markers. (C,F) Cell supernatants were collected at 24 hours and IL-2 expression was
648 analyzed by ELISA. Data represent means +/- StDev from 3-6 replicate samples from one
649 representative experiment, N=2 experiments.

650 **Figure 4. CD4 T cell proliferation is stiffness dependent and IL-2 independent.**
651 OT-II $CD4^+$ T cells were purified from lymph nodes and spleen and activated on stimulatory
652 acrylamide hydrogel surfaces with a stiffness range of 2 – 25 kPa (and plastic). Stimulatory
653 surfaces were coated with the indicated concentrations of pMHC-II together with 2 µg/ml anti-
654 CD28. (A,B) Proliferation of $CD4^+$ T cells was measured by CFSE dilution at 72 hours post
655 activation, showing profound stiffness-dependent proliferation. (A) Representative CFSE dilution
656 matrix from a single experiment. (B) Average division index from 5 independent experiments. (C)

657 Representative plots of CD25 expression as a function of CFSE dilution at 72 hours from a single
658 experiment shows that upregulation of CD25 on T cell membrane precedes proliferation. (D)
659 Average percent of T cells expressing CD25 from 5 independent experiments. (E) Division index
660 of $CD4^+$ T cells activated with or without addition of 25 U/ml of exogenous IL-2. Data in B, D, and
661 E represent averages +/- SEM from at least 3 independent experiments.

662 **Figure 5. $CD8^+$ T cell proliferation and degranulation show moderate stiffness dependency**
663 Naïve OT-I $CD8^+$ T cells were purified from lymph nodes and spleen and activated on stimulatory
664 acrylamide hydrogel surfaces with a stiffness range of 2 – 25 kPa (and plastic). Stimulatory
665 surfaces were coated with the indicated concentrations of pMHC-I together with 2 µg/ml anti-
666 CD28 (A,B) Proliferation of $CD8^+$ T cells was measured by CFSE dilution at 72 hours post
667 activation, showing only moderate stiffness-dependent proliferation. (A) Representative CFSE
668 dilution matrix from a single experiment. Note that the threshold pMHC-I concentration needed
669 to induce proliferation is very similar between the different stiffness surfaces. (B) Average
670 division index from 3 independent experiments. (C) representative plot of CD25 expression as a
671 function of CFSE dilution at 72 hours from a single experiment shows a binary stiffness response.
672 Note that with low doses of pMHC-I, only cells stimulated on very stiff substrates (25kPa or
673 plastic) survived and proliferated. Percent of live cells is given for each condition. (D) Average
674 percent of T cells expressing CD25 from 3 independent experiments. Levels of CD25 membrane
675 expression are very similar between the different substrates, probably reflecting the fact that
676 only T cells that upregulate CD25 survive. (E) Cytotoxic $CD8^+$ T cells on days 8 or 9 of culture
677 were restimulated on hydrogel surfaces with a range of pMHC-I concentrations, and
678 degranulation was measured based on surface exposure of CD107a (N=3). Data in B, D, and E
679 represent averages +/- SEM from at least 3 independent experiments.

680

681 **Figure 6. Stimulation of TCR with pMHC leads to the strongest stiffness-dependent response.**

682 OT-II $CD4^+$ T cells were stimulated on acrylamide hydrogels of different stiffnesses coated with
683 the indicated range of stimulatory ligands. Proliferation and membrane expression of CD25 were
684 measured 72 hours post activation by flow cytometry. (A,D) Stimulation with anti-CD3ε
685 antibody. (B,E) Stimulation with anti-TCRβ antibody. (C,F) Stimulation with pMHC-II. Plots show
686 the average division index or CD25 expression from 3 independent experiment. Gray areas
687 denote a similar range of stimulatory ligand molar concentrations to aid comparison.

688 **Figure 7. DC cortical stiffness acts as a costimulatory signal for T cell activation**

689 WT or $WASp^{-/-}$ BMDCs, or WT BMDCs transduced with constituently active form of WASp (CA-
690 WASp) were untreated or matured by treatment with LPS. (A) Cortical stiffness was measured
691 by AFM micro-indentation. Each data point represents an average of two stiffness
692 measurements at different locations around a single cell nucleus. Error bars denote standard
693 deviation. ***$p<0.001$, ****$p<0.0001$ calculated by an unpaired one-way ANOVA, comparing
694 mature WT with all other treatments, with post-hoc Tukey correction. (B,C) LPS-matured BMDCs
695 were pulsed with a range of $OVA_{323-339}$ peptide concentrations and co-cultured with *ex-vivo* OT-II
696 $CD4^+$ T cells for 72 hrs. Proliferation was measured by CFSE dilution. (D,E) Proliferation index
697 pooled from two independent experiments. (F-G) Division index values pooled from two
698 independent experiments. Error bars represent StDev.

699 **Figure 1 – Figure Supplement 1. Validation of hydrogel compliances.**

700 Direct AFM measurements of hydrogel compliance, validating the stiffness of hydrogels used for
701 measuring the effects of substrate compliance on DC stiffness

702 **Figure 1 – Figure Supplement 2. Indentation length in AFM measurements of DC cortical**
703 **stiffness**.

704 Indentation length was defined as the distance between initial deflection to maximal cantilever
705 displacement. (A) an example of a force curve and the extraction of the *de-facto* indentation
706 length. (B) quantification of indentation length for immature and mature DCs.

707 **Figure 3 – Figure Supplement 1. Validation of hydrogel compliances.**
708 Direct AFM measurements of hydrogel compliance, validating the stiffness of hydrogel surfaces
709 used for activation of T-cells.

710 **Figure 3 - Figure Supplement 2. Binding of stimulatory antibodies to various hydrogel surfaces**
711 Hydrogel surfaces were coated with 10 ug/ml of DyLight800 conjugated NutrAvidin
712 (ThermoFisher) for 2.5 hours, than washed 3 times with 200 µL of PBS, with 5 min incubations.
713 Imaging was done on a LI-COR Odyssey reader. (A) Fluorescence image of coated and uncoated
714 hydrogel plates (B) Quantification of mean fluorescent intensity for the center of each well. Each
715 data point represents mean +/- StDev pooled from two independent hydrogel wells.

716

717 **References**

718 Al-Alwan, M. M., Rowden, G., Lee, T. D., & West, K. A. (2001). The dendritic cell cytoskeleton is
719 critical for the formation of the immunological synapse. *J Immunol, 166*(3), 1452-1456.
720 Barnden, M. J., Allison, J., Heath, W. R., & Carbone, F. R. (1998). Defective TCR expression in
721 transgenic mice constructed using cDNA-based alpha- and beta-chain genes under the
722 control of heterologous regulatory elements. *Immunology and Cell Biology, 76*(1), 34-40.
723 doi:10.1046/j.1440-1711.1998.00709.x
724 Bashour, K. T., Gondarenko, A., Chen, H., Shen, K., Liu, X., Huse, M., . . . Kam, L. C. (2014). CD28
725 and CD3 have complementary roles in T-cell traction forces. *Proc Natl Acad Sci U S A,*
726 *111*(6), 2241-2246. doi:10.1073/pnas.1315606111
727 Basu, R., Whitlock, B. M., Husson, J., Le Floc'h, A., Jin, W., Oyler-Yaniv, A., . . . Huse, M. (2016).
728 Cytotoxic T Cells Use Mechanical Force to Potentiate Target Cell Killing. *Cell, 165*(1), 100-
729 110. doi:10.1016/j.cell.2016.01.021
730 Beel, K., Cotter, M. M., Blatny, J., Bond, J., Lucas, G., Greene, F., . . . Vandenberghe, P. (2009). A
731 LARGE KINDRED WITH X-LINKED NEUTROPENIA WITH AN I294T MUTATION OF THE
732 WISKOTT-ALDRICH SYNDROME GENE. *British journal of haematology, 144*(1), 120-126.
733 doi:10.1111/j.1365-2141.2008.07416.x
734 Blumenthal, D., & Burkhardt, J. K. (2020). Multiple actin networks coordinate
735 mechanotransduction at the immunological synapse. *J Cell Biol, 219*(2).
736 doi:10.1083/jcb.201911058
737 Bouma, G., Burns, S., & Thrasher, A. J. (2007). Impaired T-cell priming in vivo resulting from
738 dysfunction of WASp-deficient dendritic cells. *Blood, 110*(13), 4278-4284.
739 doi:10.1182/blood-2007-06-096875
740 Bouma, G., Mendoza-Naranjo, A., Blundell, M. P., de Falco, E., Parsley, K. L., Burns, S. O., &
741 Thrasher, A. J. (2011). Cytoskeletal remodeling mediated by WASp in dendritic cells is
742 necessary for normal immune synapse formation and T-cell priming. *Blood, 118*(9), 2492-
743 2501. doi:10.1182/blood-2011-03-340265
744 Bufi, N., Saitakis, M., Dogniaux, S., Buschinger, O., Bohineust, A., Richert, A., . . . Asnacios, A.
745 (2015). Human Primary Immune Cells Exhibit Distinct Mechanical Properties that Are
746 Modified by Inflammation. *Biophysical Journal, 108*(9), 2181-2190.
747 doi:10.1016/j.bpj.2015.03.047
748 Burns, S., Hardy, S. J., Buddle, J., Yong, K. L., Jones, G. E., & Thrasher, A. J. (2004). Maturation of
749 DC is associated with changes in motile characteristics and adherence. *Cell Motil*
750 *Cytoskeleton, 57*(2), 118-132. doi:10.1002/cm.10163
751 Burns, S., Thrasher, A. J., Blundell, M. P., Machesky, L., & Jones, G. E. (2001). Configuration of
752 human dendritic cell cytoskeleton by Rho GTPases, the WAS protein, and differentiation.
753 *Blood, 98*(4), 1142-1149.
754 Byfield, F. J., Reen, R. K., Shentu, T. P., Levitan, I., & Gooch, K. J. (2009). Endothelial actin and cell
755 stiffness is modulated by substrate stiffness in 2D and 3D. *J Biomech, 42*(8), 1114-1119.
756 doi:10.1016/j.jbiomech.2009.02.012
757 Calle, Y., Chou, H. C., Thrasher, A. J., & Jones, G. E. (2004). Wiskott-Aldrich syndrome protein and
758 the cytoskeletal dynamics of dendritic cells. *Journal of Pathology, 204*(4), 460-469.
759 doi:10.1002/path.1651
760 Comrie, W. A., Li, S., Boyle, S., & Burkhardt, J. K. (2015). The dendritic cell cytoskeleton promotes
761 T cell adhesion and activation by constraining ICAM-1 mobility. *J Cell Biol, 208*(4), 457-
762 473. doi:10.1083/jcb.201406120
763 Das, D. K., Feng, Y., Mallis, R. J., Li, X., Keskin, D. B., Hussey, R. E., . . . Lang, M. J. (2015). Force-
764 dependent transition in the T-cell receptor beta-subunit allosterically regulates peptide

765 discrimination and pMHC bond lifetime. *Proc Natl Acad Sci U S A, 112*(5), 1517-1522.
766 doi:10.1073/pnas.1424829112
767 Demoulin, D., Carlier, M. F., Bibette, J., & Baudry, J. (2014). Power transduction of actin filaments
768 ratcheting in vitro against a load. *Proc Natl Acad Sci U S A, 111*(50), 17845-17850.
769 doi:10.1073/pnas.1414184111
770 Discher, D. E., Janmey, P., & Wang, Y.-l. (2005). Tissue Cells Feel and Respond to the Stiffness of
771 Their Substrate. *Science, 310*(5751), 1139-1143. doi:10.1126/science.1116995
772 Doan, T., McNally, A., Thomas, R., & Steptoe, R. J. (2009). Steady-state dendritic cells continuously
773 inactivate T cells that escape thymic negative selection. *Immunol Cell Biol, 87*(8), 615-622.
774 doi:10.1038/icb.2009.46
775 Dustin, M. L. (2014). The immunological synapse. *Cancer Immunol Res, 2*(11), 1023-1033.
776 doi:10.1158/2326-6066.CIR-14-0161
777 Engler, A. J., Sen, S., Sweeney, H. L., & Discher, D. E. Matrix Elasticity Directs Stem Cell Lineage
778 Specification. *Cell, 126*(4), 677-689. doi:10.1016/j.cell.2006.06.044
779 Friedl, P., den Boer, A. T., & Gunzer, M. (2005). Tuning immune responses: diversity and
780 adaptation of the immunological synapse. *Nat Rev Immunol, 5*(7), 532-545.
781 doi:10.1038/nri1647
782 Garrett, W. S., Chen, L. M., Kroschewski, R., Ebersold, M., Turley, S., Trombetta, S., . . . Mellman,
783 I. (2000). Developmental control of endocytosis in dendritic cells by Cdc42. *Cell, 102*(3),
784 325-334.
785 Gleisner, M. A., Rosemblatt, M., Fierro, J. A., & Bono, M. R. (2011). Delivery of alloantigens via
786 apoptotic cells generates dendritic cells with an immature tolerogenic phenotype.
787 *Transplant Proc, 43*(6), 2325-2333. doi:10.1016/j.transproceed.2011.06.007
788 Gordon, J. R., Ma, Y., Churchman, L., Gordon, S. A., & Dawicki, W. (2014). Regulatory dendritic
789 cells for immunotherapy in immunologic diseases. *Front Immunol, 5*, 7.
790 doi:10.3389/fimmu.2014.00007
791 Guilliams, M., & Malissen, B. (2015). A Death Notice for In-Vitro-Generated GM-CSF Dendritic
792 Cells? *Immunity, 42*(6), 988-990. doi:10.1016/j.immuni.2015.05.020
793 Harding, F. A., McArthur, J. G., Gross, J. A., Raulet, D. H., & Allison, J. P. (1992). CD28-mediated
794 signalling co-stimulates murine T cells and prevents induction of anergy in T-cell clones.
795 *Nature, 356*(6370), 607-609. doi:10.1038/356607a0
796 Hogquist, K. A., Jameson, S. C., Heath, W. R., Howard, J. L., Bevan, M. J., & Carbone, F. R. (1994).
797 T cell receptor antagonist peptides induce positive selection. *Cell, 76*(1), 17-27.
798 doi:10.1016/0092-8674(94)90169-4
799 Hong, J., Persaud, S. P., Horvath, S., Allen, P. M., Evavold, B. D., & Zhu, C. (2015). Force-Regulated
800 In Situ TCR-Peptide-Bound MHC Class II Kinetics Determine Functions of CD4+ T Cells. *J*
801 *Immunol, 195*(8), 3557-3564. doi:10.4049/jimmunol.1501407
802 Huang, Y., Biswas, C., Klos Dehring, D. A., Sriram, U., Williamson, E. K., Li, S., . . . Burkhardt, J. K.
803 (2011). The actin regulatory protein HS1 is required for antigen uptake and presentation
804 by dendritic cells. *Journal of Immunology, 187*(11), 5952-5963.
805 doi:10.4049/jimmunol.1100870
806 Hui, K. L., Balagopalan, L., Samelson, L. E., & Upadhyaya, A. (2015). Cytoskeletal forces during
807 signaling activation in Jurkat T-cells. *Mol Biol Cell, 26*(4), 685-695. doi:10.1091/mbc.E14-
808 03-0830
809 Husson, J., Chemin, K., Bohineust, A., Hivroz, C., & Henry, N. (2011). Force generation upon T cell
810 receptor engagement. *PLoS One, 6*(5), e19680. doi:10.1371/journal.pone.0019680
811 Inaba, K., Inaba, M., Romani, N., Aya, H., Deguchi, M., Ikehara, S., . . . Steinman, R. M. (1992).
812 Generation of large numbers of dendritic cells from mouse bone marrow cultures

supplemented with granulocyte/macrophage colony-stimulating factor. *The Journal of Experimental Medicine, 176*(6), 1693-1702. doi:10.1084/jem.176.6.1693

Judokusumo, E., Tabdanov, E., Kumari, S., Dustin, M. L., & Kam, L. C. (2012). Mechanosensing in T lymphocyte activation. *Biophysical Journal, 102*(2), L5-7. doi:10.1016/j.bpj.2011.12.011

Jung, S., Unutmaz, D., Wong, P., Sano, G., De los Santos, K., Sparwasser, T., . . . Lang, R. A. (2002). In vivo depletion of CD11c+ dendritic cells abrogates priming of CD8+ T cells by exogenous cell-associated antigens. *Immunity, 17*(2), 211-220.

Kim, S. T., Takeuchi, K., Sun, Z. Y., Touma, M., Castro, C. E., Fahmy, A., . . . Reinherz, E. L. (2009). The alphabeta T cell receptor is an anisotropic mechanosensor. *J Biol Chem, 284*(45), 31028-31037. doi:10.1074/jbc.M109.052712

Lahm, H. W., & Stein, S. (1985). Characterization of recombinant human interleukin-2 with micromethods. *J Chromatogr, 326*, 357-361.

Lee, M. S., Glassman, C. R., Deshpande, N. R., Badgandi, H. B., Parrish, H. L., Uttamapinant, C., . . . Kuhns, M. S. (2015). A Mechanical Switch Couples T Cell Receptor Triggering to the Cytoplasmic Juxtamembrane Regions of CD3zetazeta. *Immunity, 43*(2), 227-239. doi:10.1016/j.immuni.2015.06.018

Levitsky, H. I., Montgomery, J., Ahmadzadeh, M., Staveley-O'Carroll, K., Guarnieri, F., Longo, D. L., & Kwak, L. W. (1996). Immunization with granulocyte-macrophage colony-stimulating factor-transduced, but not B7-1-transduced, lymphoma cells primes idiotype-specific T cells and generates potent systemic antitumor immunity. *J Immunol, 156*(10), 3858-3865.

Li, Y. C., Chen, B. M., Wu, P. C., Cheng, T. L., Kao, L. S., Tao, M. H., . . . Roffler, S. R. (2010). Cutting Edge: mechanical forces acting on T cells immobilized via the TCR complex can trigger TCR signaling. *J Immunol, 184*(11), 5959-5963. doi:10.4049/jimmunol.0900775

Liu, B., Chen, W., Evavold, B. D., & Zhu, C. (2014). Accumulation of dynamic catch bonds between TCR and agonist peptide-MHC triggers T cell signaling. *Cell, 157*(2), 357-368. doi:10.1016/j.cell.2014.02.053

Lo, C.-M., Wang, H.-B., Dembo, M., & Wang, Y.-l. Cell Movement Is Guided by the Rigidity of the Substrate. *Biophysical Journal, 79*(1), 144-152. doi:10.1016/S0006-3495(00)76279-5

Lutz, M. B., Inaba, K., Schuler, G., & Romani, N. (2016). Still Alive and Kicking: In-Vitro-Generated GM-CSF Dendritic Cells! *Immunity, 44*(1), 1-2. doi:10.1016/j.immuni.2015.12.013

Ma, Z., Janmey, P. A., & Finkel, T. H. (2008). The receptor deformation model of TCR triggering. *FASEB J, 22*(4), 1002-1008. doi:10.1096/fj.07-9331hyp

McAdam, A. J., Schweitzer, A. N., & Sharpe, A. H. (1998). The role of B7 co-stimulation in activation and differentiation of CD4+ and CD8+ T cells. *Immunol Rev, 165*, 231-247. doi:10.1111/j.1600-065x.1998.tb01242.x

Mellman, I., & Steinman, R. M. (2001). Dendritic cells: specialized and regulated antigen processing machines. *Cell, 106*(3), 255-258.

Na, Y. R., Jung, D., Gu, G. J., & Seok, S. H. (2016). GM-CSF Grown Bone Marrow Derived Cells Are Composed of Phenotypically Different Dendritic Cells and Macrophages. *Mol Cells, 39*(10), 734-741. doi:10.14348/molcells.2016.0160

O'Connor, R. S., Hao, X., Shen, K., Bashour, K., Akimova, T., Hancock, W. W., . . . Milone, M. C. (2012). Substrate rigidity regulates human T cell activation and proliferation. *Journal of Immunology, 189*(3), 1330-1339. doi:10.4049/jimmunol.1102757

Oakes, P. W., Patel, D. C., Morin, N. A., Zitterbart, D. P., Fabry, B., Reichner, J. S., & Tang, J. X. (2009). Neutrophil morphology and migration are affected by substrate elasticity. *Blood, 114*(7), 1387-1395. doi:10.1182/blood-2008-11-191445

Pelham, R. J., & Wang, Y.-l. (1997). Cell locomotion and focal adhesions are regulated by substrate flexibility. *Proceedings of the National Academy of Sciences, 94*(25), 13661-13665.

862 Pryshchep, S., Zarnitsyna, V. I., Hong, J., Evavold, B. D., & Zhu, C. (2014). Accumulation of serial
863 forces on TCR and CD8 frequently applied by agonist antigenic peptides embedded in
864 MHC molecules triggers calcium in T cells. *J Immunol, 193*(1), 68-76.
865 doi:10.4049/jimmunol.1303436
866 Renkawitz, J., Schumann, K., Weber, M., Lammermann, T., Pflicke, H., Piel, M., . . . Sixt, M. (2009).
867 Adaptive force transmission in amoeboid cell migration. *Nat Cell Biol, 11*(12), 1438-1443.
868 doi:10.1038/ncb1992
869 Saitakis, M., Dogniaux, S., Goudot, C., Bufi, N., Asnacios, S., Maurin, M., . . . Hivroz, C. (2017).
870 Different TCR-induced T lymphocyte responses are potentiated by stiffness with variable
871 sensitivity. *Elife, 6*. doi:10.7554/eLife.23190
872 Salbreux, G., Charras, G., & Paluch, E. (2012). Actin cortex mechanics and cellular morphogenesis.
873 *Trends Cell Biol, 22*(10), 536-545. doi:10.1016/j.tcb.2012.07.001
874 Sawicka, A., Babataheri, A., Dogniaux, S., Barakat, A. I., Gonzalez-Rodriguez, D., Hivroz, C., &
875 Husson, J. (2017). Micropipette force probe to quantify single-cell force generation:
876 application to T-cell activation. *Mol Biol Cell, 28*(23), 3229-3239. doi:10.1091/mbc.E17-
877 06-0385
878 Snapper, S. B., Rosen, F. S., Mizoguchi, E., Cohen, P., Khan, W., Liu, C. H., . . . Alt, F. W. (1998).
879 Wiskott-Aldrich syndrome protein-deficient mice reveal a role for WASP in T but not B cell
880 activation. *Immunity, 9*(1), 81-91.
881 Solon, J., Levental, I., Sengupta, K., Georges, P. C., & Janmey, P. A. Fibroblast Adaptation and
882 Stiffness Matching to Soft Elastic Substrates. *Biophysical Journal, 93*(12), 4453-4461.
883 doi:10.1529/biophysj.106.101386
884 Sun, Z. J., Kim, K. S., Wagner, G., & Reinherz, E. L. (2001). Mechanisms contributing to T cell
885 receptor signaling and assembly revealed by the solution structure of an ectodomain
886 fragment of the CD3 epsilon gamma heterodimer. *Cell, 105*(7), 913-923.
887 doi:10.1016/s0092-8674(01)00395-6
888 Swamy, M., Beck-Garcia, K., Beck-Garcia, E., Hartl, F. A., Morath, A., Yousefi, O. S., . . . Schamel,
889 W. W. (2016). A Cholesterol-Based Allostery Model of T Cell Receptor Phosphorylation.
890 *Immunity, 44*(5), 1091-1101. doi:10.1016/j.immuni.2016.04.011
891 Taniuchi, I., Kitamura, D., Maekawa, Y., Fukuda, T., Kishi, H., & Watanabe, T. (1995). Antigen-
892 receptor induced clonal expansion and deletion of lymphocytes are impaired in mice
893 lacking HS1 protein, a substrate of the antigen-receptor-coupled tyrosine kinases. *EMBO*
894 *J, 14*(15), 3664-3678.
895 Tee, S. Y., Fu, J., Chen, C. S., & Janmey, P. A. (2011). Cell shape and substrate rigidity both regulate
896 cell stiffness. *Biophys J, 100*(5), L25-27. doi:10.1016/j.bpj.2010.12.3744
897 Trappmann, B., Gautrot, J. E., Connelly, J. T., Strange, D. G. T., Li, Y., Oyen, M. L., . . . Huck, W. T. S.
898 (2012). Extracellular-matrix tethering regulates stem-cell fate. *Nature Materials, 11*, 642.
899 doi:10.1038/nmat3339
900 van Helden, S. F., Oud, M. M., Joosten, B., Peterse, N., Figdor, C. G., & van Leeuwen, F. N. (2008).
901 PGE2-mediated podosome loss in dendritic cells is dependent on actomyosin contraction
902 downstream of the RhoA-Rho-kinase axis. *J Cell Sci, 121*(Pt 7), 1096-1106.
903 doi:10.1242/jcs.020289
904 Vargas, P., Maiuri, P., Bretou, M., Saez, P. J., Pierobon, P., Maurin, M., . . . Lennon-Dumenil, A. M.
905 (2016). Innate control of actin nucleation determines two distinct migration behaviours
906 in dendritic cells. *Nat Cell Biol, 18*(1), 43-53. doi:10.1038/ncb3284
907 West, M. A., Prescott, A. R., Eskelinen, E. L., Ridley, A. J., & Watts, C. (2000). Rac is required for
908 constitutive macropinocytosis by dendritic cells but does not control its downregulation.
909 *Curr Biol, 10*(14), 839-848.

910 Westerberg, L. S., Meelu, P., Baptista, M., Eston, M. A., Adamovich, D. A., Cotta-de-Almeida, V., . .
911 . . Snapper, S. B. (2010). Activating WASP mutations associated with X-linked neutropenia
912 result in enhanced actin polymerization, altered cytoskeletal responses, and genomic
913 instability in lymphocytes. *The Journal of Experimental Medicine, 207*(6), 1145-1152.
914 doi:10.1084/jem.20091245
915 Wu, P. H., Aroush, D. R., Asnacios, A., Chen, W. C., Dokukin, M. E., Doss, B. L., . . . Wirtz, D. (2018).
916 A comparison of methods to assess cell mechanical properties. *Nat Methods, 15*(7), 491-
917 498. doi:10.1038/s41592-018-0015-1
918 Xu, C., Gagnon, E., Call, M. E., Schnell, J. R., Schwieters, C. D., Carman, C. V., . . . Wucherpfennig,
919 K. W. (2008). Regulation of T cell receptor activation by dynamic membrane binding of
920 the CD3epsilon cytoplasmic tyrosine-based motif. *Cell, 135*(4), 702-713.
921 doi:10.1016/j.cell.2008.09.044
922 Yamashiro, S. (2012). Functions of fascin in dendritic cells. *Crit Rev Immunol, 32*(1), 11-21.

923

Blumenthal et al. “T-cell priming is enhanced by maturation-dependent stiffening of the dendritic cell cortex”

Figure 1

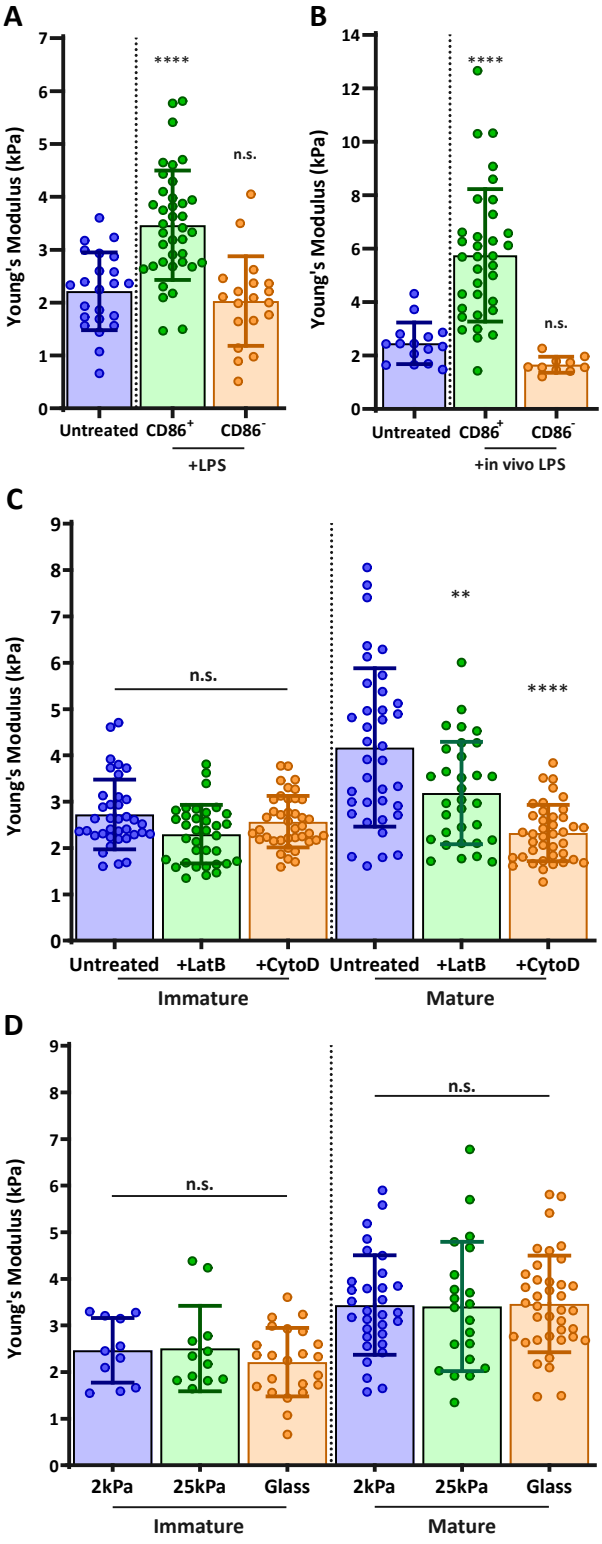

Blumenthal et al. “T-cell priming is enhanced by maturation-dependent stiffening of the dendritic cell cortex”

Figure 2

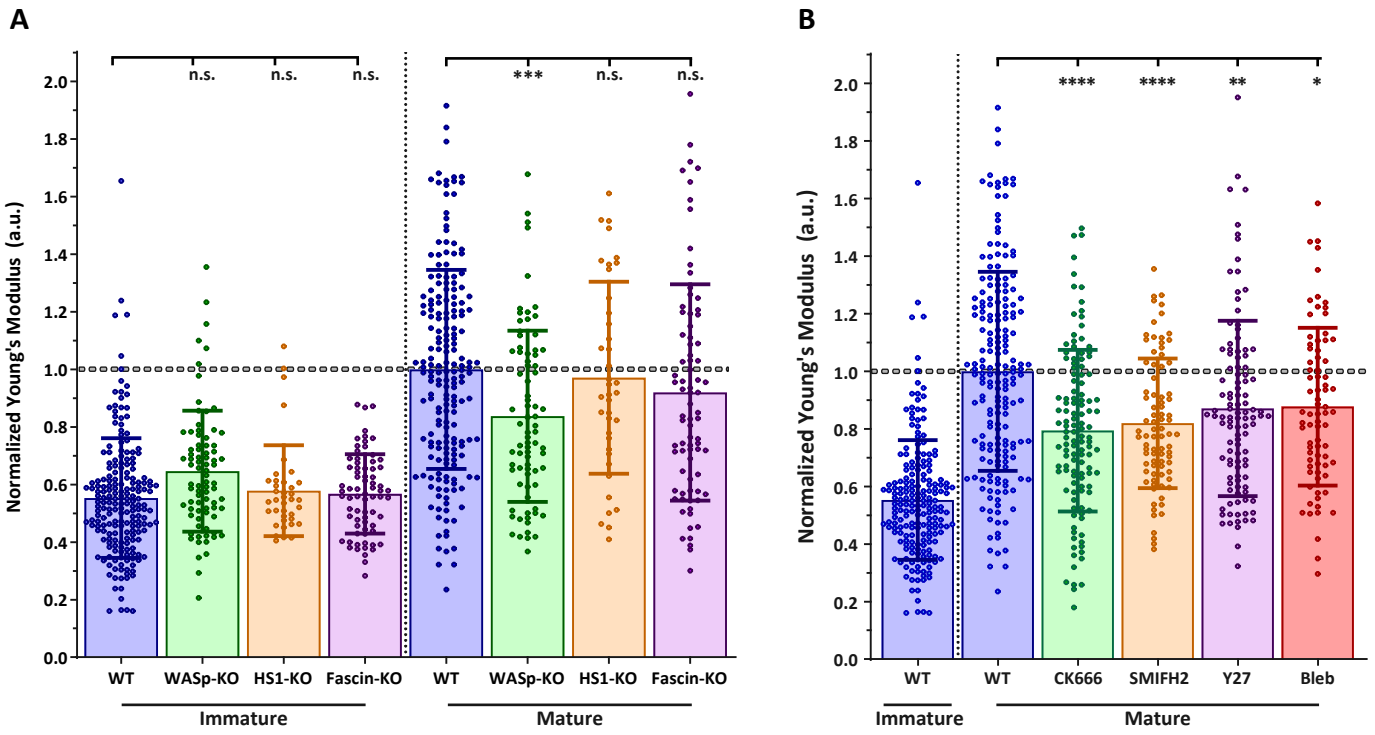

Blumenthal et al. “T-cell priming is enhanced by maturation-dependent stiffening of the dendritic cell cortex”

Figure 3

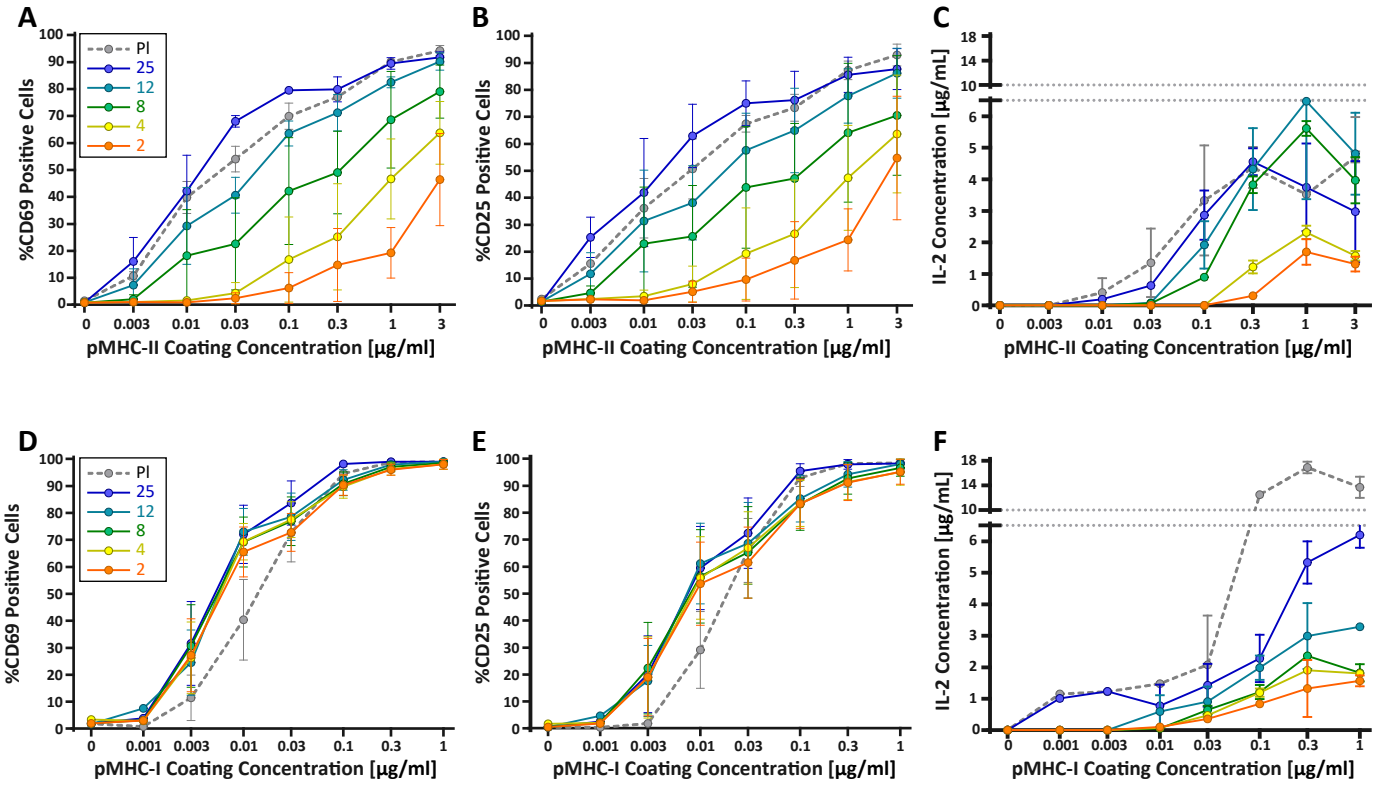

Blumenthal et al. "T-cell priming is enhanced by maturation-dependent stiffening of the dendritic cell cortex"

Figure 4

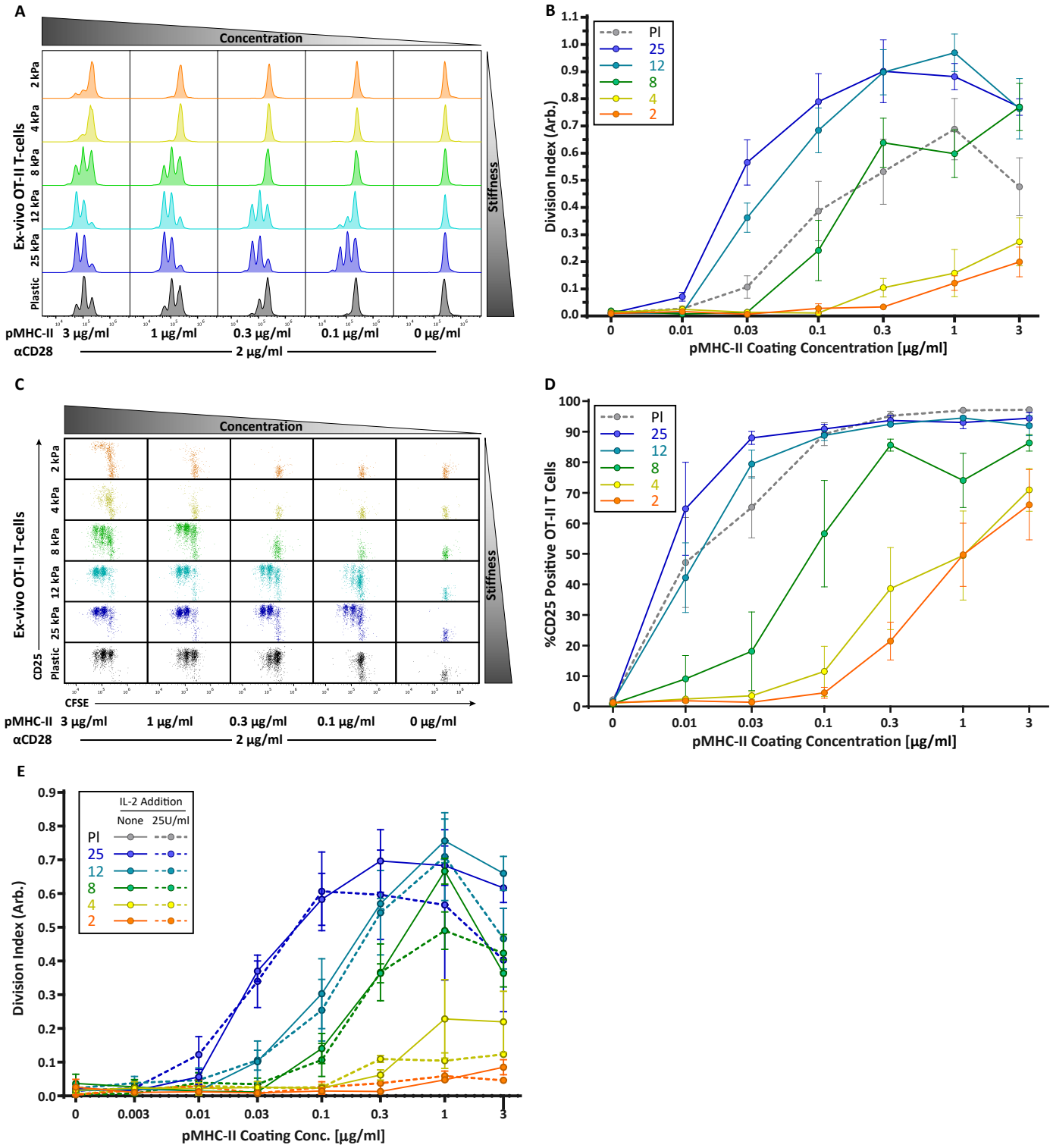

Blumenthal et al. "T-cell priming is enhanced by maturation-dependent stiffening of the dendritic cell cortex"

Figure 5

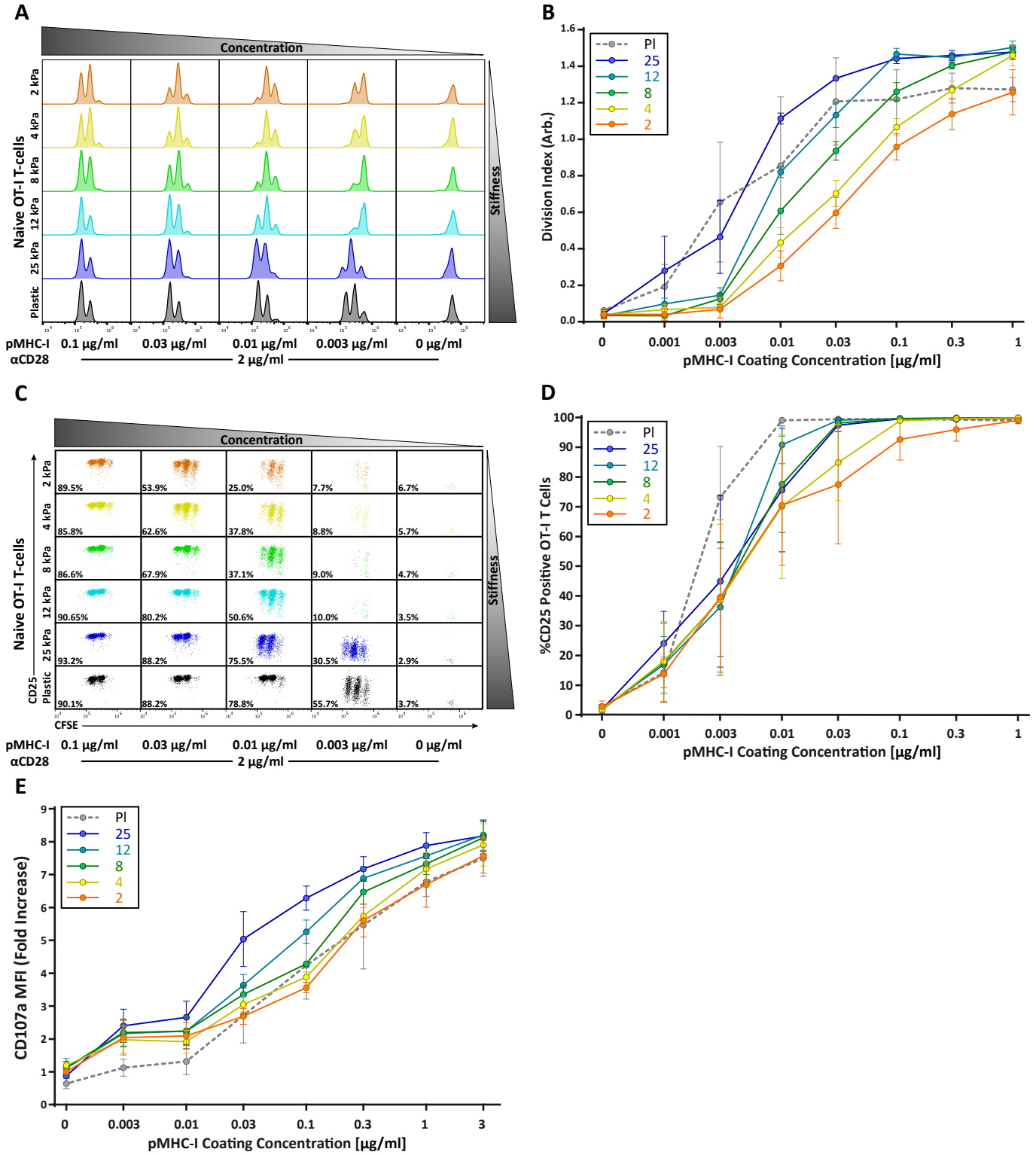

Blumenthal et al. “T-cell priming is enhanced by maturation-dependent stiffening of the dendritic cell cortex”

Figure 6

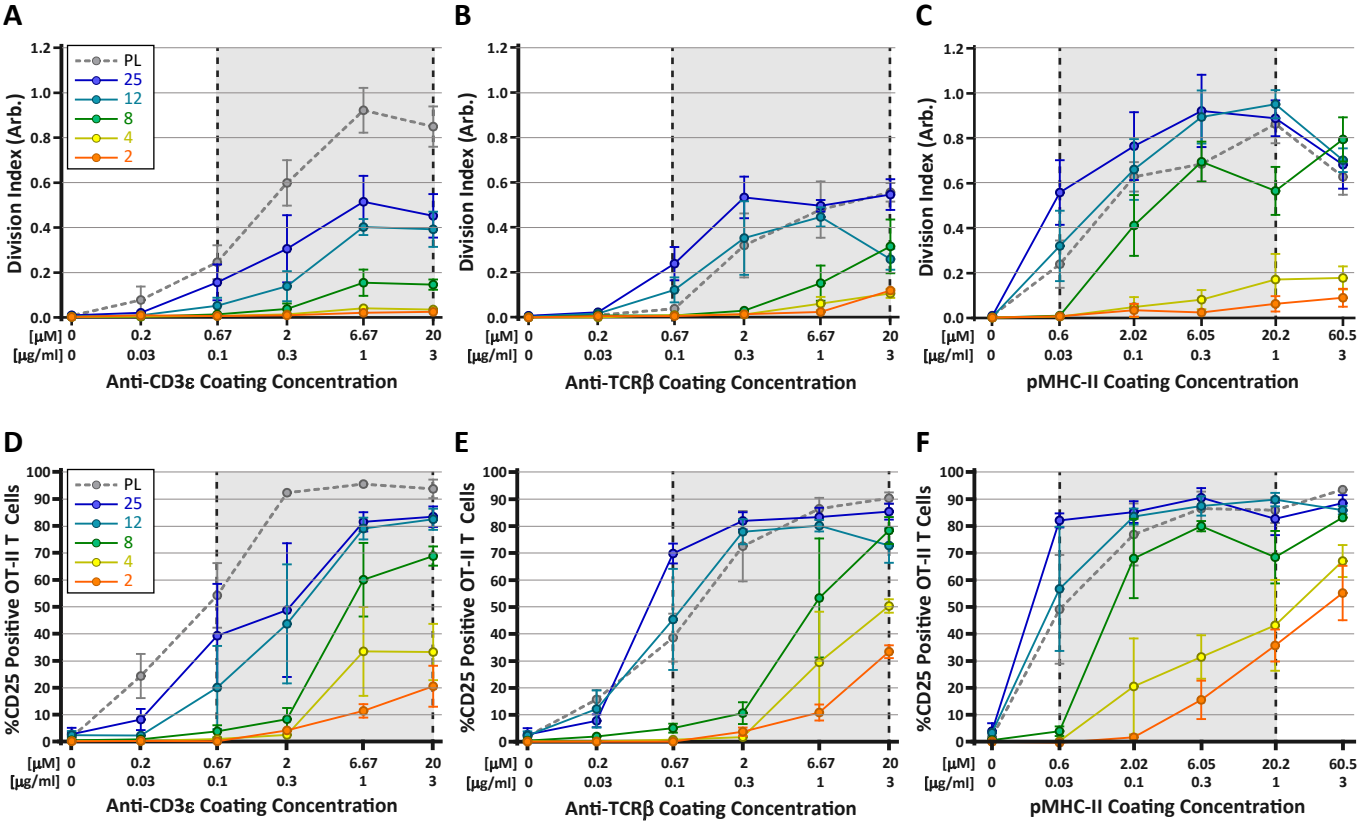

Blumenthal et al. “T-cell priming is enhanced by maturation-dependent stiffening of the dendritic cell cortex”
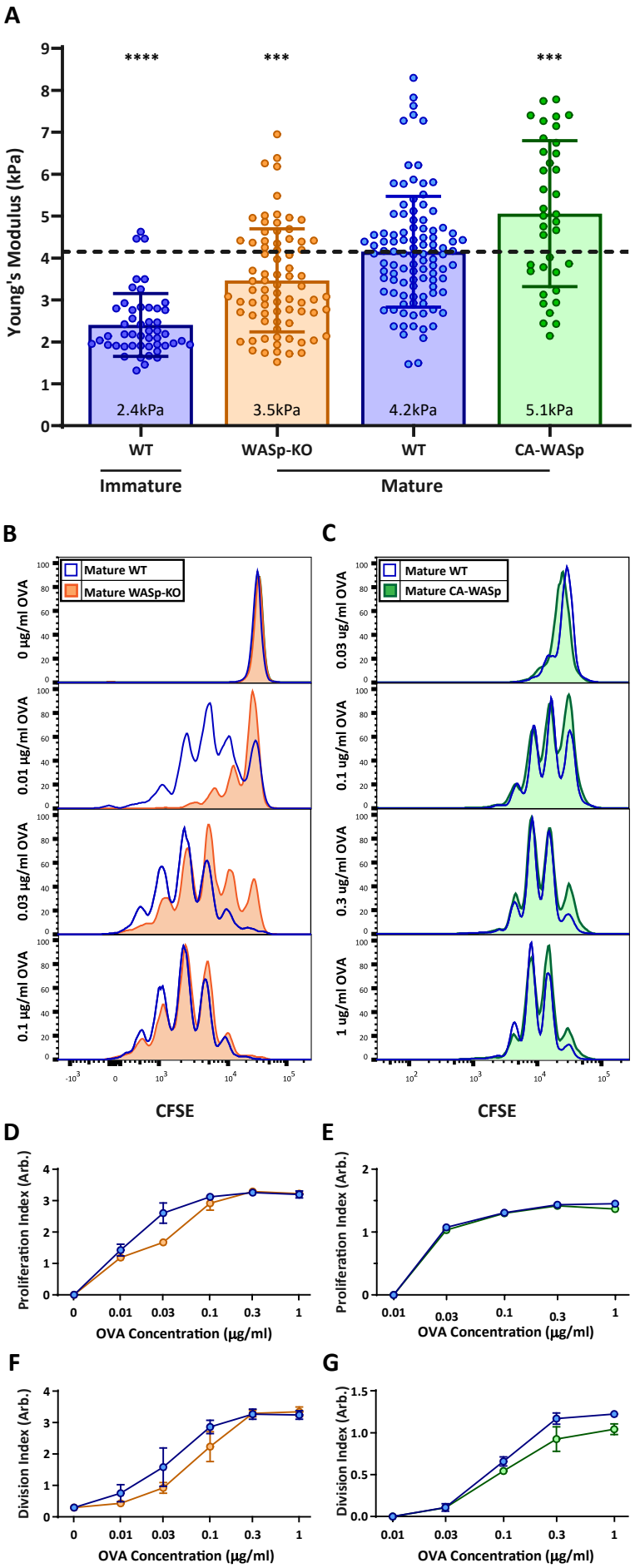
Figure 7